Annals of Actuarial Science (2026), **20**, pp. 439–472
doi:10.1017/S174849952610027X

ORIGINAL RESEARCH PAPER

State-space dynamic functional regression for multicurve fixed income spread analysis and stress testing

Peilun He[1,2], Gareth W. Peters[2], Nino Kordzakhia[3] and Pavel V. Shevchenko[1]

[1]Actuarial Studies and Business Analytics, Macquarie Business School, Macquarie University, Australia; [2]Statistics and Applied Probability, University of California Santa Barbara, Santa Barbara, USA; and [3]School of Mathematical and Physical Sciences, Macquarie University, Australia
Corresponding author: Pavel V. Shevchenko; Email: pavel.shevchenko@mq.edu.au

(Received 10 May 2025; revised 05 December 2025; accepted 10 March 2026; first published online 14 April 2026)

Abstract

The Nelson–Siegel model is widely used in fixed income markets to produce yield curve dynamics. The multiple time-dependent parameter model conveniently addresses the level, slope, and curvature dynamics of the yield curves. In this study, we present a novel state-space functional regression model that incorporates a dynamic Nelson–Siegel (DNS) model and functional regression formulations applied to a multi-economy setting. This framework offers distinct advantages in explaining the relative spreads in yields between a reference economy and a response economy. To address the inherent challenges of model calibration, a kernel principal component analysis is employed to transform the representation of functional regression into a finite-dimensional, tractable estimation problem. A comprehensive empirical analysis is conducted to assess the efficacy of the functional regression approach, including an in-sample performance comparison with the DNS model. We conducted the stress testing analysis of the yield curves' term structure within a dual economy framework. The bond ladder portfolio was examined through a case study focused on spread modeling using historical data for US Treasury and UK bonds.

Keywords: Functional regression; Nelson–Siegel model; state-space model; yield curve

1. Introduction

In global fixed income markets, bond yields serve as barometers of economic conditions, offering insights into risk assessment, valuation, and investment strategy. In the insurance sector, interest rates are crucial for pricing and managing products such as life insurance (Gaillardetz, 2008; Bernard et al., 2005), annuities (Fontana & Rotondi, 2023; Günther & Hieber, 2024), and optimal investment strategies (Han & Hung, 2017; Wang & Li, 2018; Peng & Li, 2023). A persistent challenge is the phenomenon of yield curve inversion – where short-term yields exceed long-term yields – often signaling economic recession. Understanding the determinants of such adverse yield movements is vital for informed policy and portfolio decisions.

Research on the term structure of interest rates has evolved substantially over the past decades, following two main modeling paradigms. The first is the family of no-arbitrage models, such as Hull and White (1990) and Heath *et al.* (1992), which ensure consistency with market prices through dynamic arbitrage-free frameworks. The second comprises equilibrium term structure models, including those of Vasicek (1977), Cox *et al.* (1985), and Duffie and Kan (1996), which derive interest rate dynamics from economic fundamentals. A detailed overview of these models is provided in Cairns (2004).

© The Author(s), 2026. Published by Cambridge University Press on behalf of The Institute and Faculty of Actuaries. This is an Open Access article, distributed under the terms of the Creative Commons Attribution licence (https://creativecommons.org/licenses/by/4.0/), which permits unrestricted re-use, distribution and reproduction, provided the original article is properly cited.

https://doi.org/10.1017/S174849952610027X Published online by Cambridge University Press

Whilst these models were typically derived based on continuous time stochastic diffusion models (s.d.e's), there were, in parallel, classes of models developed in discrete time econometrics settings. Such approaches formulate term structure dynamics via state-space modeling and regression methods. Dobbie and Wilkie (1978) introduced an exponential model representing yields as a sum of two exponentials, a framework that became widely used in fixed income markets. Nelson and Siegel (1987) proposed the parsimonious Nelson–Siegel model, capturing the level, slope, and curvature of the yield curve. Svensson (1994) extended it by adding a fourth term for greater flexibility, while Cairns (1998) refined these models with additional exponential terms to mitigate instability issues noted in Dobbie and Wilkie (1978) and Svensson (1994). These extensions were applied to the UK and German bond markets in Cairns (1998) and Cairns and Pritchard (2001), respectively.

Diebold and Li (2006) introduced autoregressive dynamics into the Nelson–Siegel model, improving long-horizon forecasts of US Treasury yields. Subsequent studies linked macroeconomic variables – capacity utilization, the federal funds rate, and inflation – to yield curve factors (Diebold et al., 2006), and extended the model to a global multi-economy setting (Diebold et al., 2008). Further developments included time-varying loadings and GARCH errors (Koopman et al., 2010), applications to corporate yields (Yu & Zivot, 2011), and assessments of parameter stability (Wahlstrøm et al., 2022).

Recent advances include quantile-based modeling for economic shocks (Iacopini et al., 2024), arbitrage-free formulations (Eghbalzadeh et al., 2024; Fontana et al., 2025), and stochastic process approaches for bond portfolios (Andersson & Lagerås, 2013). Comparisons with affine models are discussed in Filipovic (1999), while comprehensive reviews are provided in Diebold and Rudebusch (2013). Furthermore, the implementations of the widely used single curve dynamics via Nelson–Siegel model and its extensions are available in popular R ("YieldCurve" and "NMOF" packages, see Guirreri (2010) and Schumann (2016), respectively) and Python ("PyCurve").

Despite its flexibility, the Nelson–Siegel family faces two key limitations: (i) reduced accuracy for long-maturity bonds, as shown by Christensen *et al.* (2009) and Dubecq and Gourieroux (2011), and (ii) the lack of inter-economy dependence. The latter was partially addressed in the dynamic Nelson–Siegel (DNS) state-space setting via probabilistic PCA factors capturing global and cross-country relationships (Toczydlowska & Peters, 2018).

Despite all these developments in term structure dynamic modeling, all modeling approaches face challenges in capturing the joint dynamics of yield curves across economies and maturities. This motivates the development of more flexible frameworks capable of incorporating functional, temporal, and cross-market dependencies, which form the focus of this study.

1.1 Contributions

This study advances yield curve modeling and risk assessment through both methodological and applied innovations.

First, we propose a novel *state-space functional regression model* that integrates the DNS framework with functional regression. This hybrid approach jointly models time series and functional dependencies, improving the flexibility and accuracy of yield curve estimation. Estimation challenges are addressed using kernel principal component analysis (kPCA), which maps the infinite-dimensional functional regression problem into a tractable finite-dimensional estimation problem.

Second, we apply the model to yield curves from eight economies, benchmarking its performance against the traditional DNS model. By incorporating relative spreads with respect to US Treasury yields, the proposed framework achieves robust in-sample estimation and captures long-end yield dynamics more effectively across all response markets.

Third, we perform *stress testing* to evaluate inter-market dependencies under extreme conditions. Two shocks – temporary (short-term disruptions) and permanent (structural changes) – are

https://doi.org/10.1017/S174849952610027X Published online by Cambridge University Press

applied to US Treasury yields to assess their propagation to the UK market. This analysis highlights both immediate and persistent effects of US shocks, providing insights into systemic risk transmission and resilience of bond markets.

Finally, we construct a bond ladder portfolio using 12-month out-of-sample forecasts, quantifying potential losses via the 5% value-at-risk (VaR) under various stress scenarios. This enables a comprehensive evaluation of yield curve risks from an investment strategy perspective.

1.2 Notations and structures

Throughout this paper, we adopt the following multicurve notations: $Y_t(\tau_i)$ represents the complete bond yields of the response country (dependent curve observation process to be modeled), and $Y_t^{(r)}(\tau_i)$ denotes the complete bond yields of the reference country, i.e., the independent curve dynamic that characterizes part of the explanatory factors for the response country, where $t \in \{1, 2, \ldots, T\}$ represents the current time, and $\tau_1 < \tau_2 < \ldots < \tau_N$ are times to maturity. Both $Y_t(\tau_i)$ and $Y_t^{(r)}(\tau_i)$ are annualized rates. In the real data over time, we may not observe a complete term structure, so we denote by $\tilde{Y}_t(\tau_i)$ and $\tilde{Y}_t^{(r)}(\tau_i)$ the observed data which may contain missing values in the term structure over time. Additionally, we use $F_{i,t}$ for $i \in \{1, 2, 3\}$ to denote Nelson–Siegel factors and $U_{j,t}$ for $j \in \{1, \ldots, Q\}$ to represent US factors extracted using kPCA. Bold font is used to represent matrices and vectors. $\boldsymbol{Y} = \{Y_t(\tau_i)\}$ is the matrix of all observations of the response country, while $\boldsymbol{Y}_t^\top$ and $\boldsymbol{Y}(\tau_i)$ are the t-th row and i-th column of $\boldsymbol{Y}$, respectively. Similarly, we define $\boldsymbol{Y}^{(r)} = \{Y_t^{(r)}(\tau_i)\}$ as the matrix of all observations of the reference country, and $\boldsymbol{Y}_t^{(r)\top}$ and $\boldsymbol{Y}^{(r)}(\tau_i)$ are the t-th row and i-th column of $\boldsymbol{Y}^{(r)}$.

This paper is structured to provide a comprehensive exploration of the DNS functional regression (DNS-FR) model and its applications. In Section 3, we first define the DNS model, and then extend it by adding a functional regression component to incorporate the relative spread of a reference country. Section 4 focuses on the functional transformation that transfers the functional regression to a finite-dimensional estimation problem through kPCA. Subsequently, in Sections 5 and 6, we delve into the estimation and forecasting methods, respectively. Section 7 offers an overview of the data utilized in this study. Empirical results, including the comparison of the DNS model and the DNS-FR model in terms of in-sample estimation and out-of-sample forecasting, stress testing, and a case study of a bond ladder portfolio, are presented in Section 8. Finally, Section 9 concludes.

2. Background on multicurve modeling

Previous approaches to multicurve modeling differ markedly from the framework proposed in this paper. In Diebold *et al.* (2008), multiple government bond yields were linked through an unobserved synthetic "global" yield curve – an artificial construct never used in the estimation stage. Their model employed only two factors (level and slope), with the latent global factors driving the dynamics of each country's two-factor Nelson–Siegel process. In essence, this structure introduces common stochastic dependence across countries, but the synthetic global curve itself is redundant, as it serves no direct empirical role. Specifically, the yield of country k at maturity τ_i is given by

$$Y_t^{(k)}(\tau_i) = L_t^{(k)} + S_t^{(k)} \left(\frac{1 - e^{-\lambda_k \tau_i}}{\lambda_k \tau_i} \right) + \nu_t^{(k)}(\tau_i), \tag{1}$$

where $L_t^{(k)}$ and $S_t^{(k)}$ denote the level and slope factors, and $\nu_t^{(k)}(\tau_i)$ is the measurement error. The global latent factors evolve as

https://doi.org/10.1017/S174849952610027X Published online by Cambridge University Press

$$\begin{bmatrix} L_t \\ S_t \end{bmatrix} = \begin{bmatrix} \Phi_{11} & \Phi_{12} \\ \Phi_{21} & \Phi_{22} \end{bmatrix} \begin{bmatrix} L_{t-1} \\ S_{t-1} \end{bmatrix} + \begin{bmatrix} \epsilon_{L,t} \\ \epsilon_{S,t} \end{bmatrix}. \tag{2}$$

Each country's local factors are linearly related to the global factors:

$$L_t^{(k)} = \alpha_L^{(k)} + \beta_L^{(k)} L_t + \epsilon_{L,t}^{(k)}, \tag{3}$$

$$S_t^{(k)} = \alpha_S^{(k)} + \beta_S^{(k)} S_t + \epsilon_{S,t}^{(k)}, \tag{4}$$

where the idiosyncratic components follow AR(1) dynamics:

$$\begin{bmatrix} \epsilon_{L,t}^{(k)} \\ \epsilon_{S,t}^{(k)} \end{bmatrix} = \begin{bmatrix} \Psi_{11}^{(k)} & \Psi_{12}^{(k)} \\ \Psi_{21}^{(k)} & \Psi_{22}^{(k)} \end{bmatrix} \begin{bmatrix} \epsilon_{L,t-1}^{(k)} \\ \epsilon_{S,t-1}^{(k)} \end{bmatrix} + \begin{bmatrix} \eta_{L,t}^{(k)} \\ \eta_{S,t}^{(k)} \end{bmatrix}. \tag{5}$$

Combining these components yields

$$\begin{aligned} Y_t^{(k)}(\tau_i) = {} & \alpha_L^{(k)} + \alpha_S^{(k)} \left(\frac{1 - e^{-\lambda_k \tau_i}}{\lambda_k \tau_i} \right) + \epsilon_{L,t}^{(k)} + \epsilon_{S,t}^{(k)} \left(\frac{1 - e^{-\lambda_k \tau_i}}{\lambda_k \tau_i} \right) \\ & + \beta_L^{(k)} L_t + \beta_S^{(k)} \left(\frac{1 - e^{-\lambda_k \tau_i}}{\lambda_k \tau_i} \right) S_t + \nu_t^{(k)}(\tau_i), \end{aligned} \tag{6}$$

where $Y_t^{(k)}(\tau_i)$ depends on global factors (L_t, S_t) and country-specific idiosyncratic terms $\epsilon_{L,t}^{(k)}, \epsilon_{S,t}^{(k)}$.

Although Diebold *et al.* (2008) discuss a "global yield curve," it is never estimated or observed, serving only as a theoretical coupling device. Without data for calibration, parameters such as λ or the error covariance of this synthetic curve remain speculative:

$$Y_t^{global}(\tau_i) = L_t + S_t \left(\frac{1 - e^{\lambda \tau_i}}{\lambda \tau_i} \right) + V_t(\tau_i), \tag{7}$$

where $V_t(\tau_i)$ denotes noise.

In contrast, our proposed framework dispenses with synthetic constructs. We use an *observed reference curve* – the US Treasury yield curve – to extract functional factors that capture both tenor and temporal dependencies. This enables direct estimation and forecasting.

3. Proposed dynamic Nelson–Siegel functional regression model

We model the complete bootstrapped bond yields $Y_t(\tau_i)$ at time t with time to maturity τ_i (in months) for a set $\{\tau_1, \ldots, \tau_N\}$ as follows:

$$\begin{aligned} Y_t(\tau_i) | Y_t^{(r)}(\tau_{1:N}) = {} & \underbrace{F_{1,t} + F_{2,t} \left(\frac{1 - e^{-\lambda \tau_i}}{\lambda \tau_i} \right) + F_{3,t} \left(\frac{1 - e^{-\lambda \tau_i}}{\lambda \tau_i} - e^{-\lambda \tau_i} \right)}_{\text{Nelson-Siegel model}} \\ & + \underbrace{\int_0^{\tau_N} \gamma_i(s) Y_t^{(r)}(s) ds}_{\text{Functional regression model}} + \epsilon_t(\tau_i) \end{aligned} \tag{8}$$

$$F_{j,t} = \psi_{j,0} + \psi_{j,1} F_{j,t-1} + \eta_{j,t}, \quad j \in \{1, 2, 3\}. \tag{9}$$

Here, τ_N is the maximum maturity of the reference country's bonds. $Y_t^{(r)}(\tau_{1:N})$ is the yield curve of reference country with maturities from τ_1 to τ_N. The parameter λ governs the decay rate.

https://doi.org/10.1017/S174849952610027X Published online by Cambridge University Press

$\gamma_i(s)$ represents the functional coefficient. $\psi_{j,0} \in \mathbb{R}$ and $\psi_{j,1} \in (-1, 1)$ are parameters to be estimated. $\epsilon_t(\tau_i)$ and $\eta_{j,t}$ are independent and identically distributed normal noises. We will discuss the structures of the covariance matrices considered for both $\epsilon_t(\tau_i)$ and $\eta_{j,t}$ later in Section 4.

As demonstrated, this model consists of two parts: a Nelson–Siegel model and a functional regression component. In Section 3.1, we first introduce the Nelson–Siegel model, and then in Section 3.2, we extend it by incorporating a functional regression component that captures the relative spread of a reference country's bonds.

3.1 Dynamic Nelson–Siegel model

We begin by introducing the latent three-factor model for the yield curve, initially proposed in Nelson and Siegel (1987) and extended in Diebold and Li (2006) to allow time-varying factors. The efficiency of this model has been demonstrated in numerous previous works, such as Diebold *et al.* (2008), Yu and Zivot (2011), and Karimalis *et al.* (2017). The Diebold and Li (Diebold & Li, 2006) formulation for the yield curve is given as:

$$Y_t(\tau_i) = F_{1,t} + F_{2,t}\left(\frac{1 - e^{-\lambda\tau_i}}{\lambda\tau_i}\right) + F_{3,t}\left(\frac{1 - e^{-\lambda\tau_i}}{\lambda\tau_i} - e^{-\lambda\tau_i}\right) + \tilde{\epsilon}_t(\tau_i), \tag{10}$$

and

$$F_{j,t} = \psi_{j,0} + \psi_{j,1}F_{j,t-1} + \tilde{\eta}_{j,t}, \quad j \in \{1, 2, 3\} \tag{11}$$

for $i \in \{1, 2, \ldots, N\}$ and $t \in \{1, 2, \ldots, T\}$. Here, $F_{1,t}, F_{2,t}, F_{3,t}$ are three latent factors typically interpreted as level, slope, and curvature. The parameter λ determines the rate of exponential decay. $\tilde{\epsilon}_t(\tau_i)$ and $\tilde{\eta}_{j,t}$ are independent and identically distributed normal noises for the measurement and state equations, respectively. Additionally, we assume that all three factors $F_{j,t}$ are uncorrelated. Given the dynamic nature of the hidden factors and for consistency with other works, we refer to this model as the DNS model.

The loading on the first factor $F_{1,t}$ is always 1 and is usually called the level. It affects all yields equally, and thus it is viewed as a long-term factor. The loading on the second factor $F_{2,t}$ is $(1 - e^{-\lambda\tau_i})/(\lambda\tau_i)$, which starts from 1 and then decays monotonically to 0 as maturity goes to infinity, hence its called the slope or short-term factor. The loading on the third factor $F_{3,t}$ is $(1 - e^{-\lambda\tau_i})/(\lambda\tau_i) - e^{-\lambda\tau_i}$. It starts from 0, first increases, and then decays to 0 again. Therefore, it contributes mostly to medium maturities and is called the curvature or medium-term factor. Figure 1 shows the factor loadings with a fixed $\lambda = 0.0609$ as in Diebold and Li (2006).

3.2 Functional regression representation with missing data

To address the limitation that the DNS model does not account for conditional relationships between different economies, we extend the DNS model by incorporating a functional regression component into the measurement equation. In recent years, functional data analysis (FDA) has gained popularity in time series modeling. In Hyndman and Shang (2009), such an approach was pioneered by introducing a weighted functional principal component regression method designed for forecasting functional time series. They successfully applied this method to Australian fertility rate data, representing time series curves as a finite sum of weighted hidden factors. Building on this methodology, Hays *et al.* (2012) introduced the functional dynamic factor model, which estimates both the hidden factor time series and the functional factor loadings simultaneously. This approach was applied to US Treasury yields, demonstrating superior performance compared to the DNS model. In a related study, Martınez-Hernández *et al.* (2022) proposed a nonparametric three-factor model, showing that the estimated factor loadings align with the level, slope, and curvature of the Nelson–Siegel model, highlighting the versatility and adaptability of FDA in

https://doi.org/10.1017/S174849952610027X Published online by Cambridge University Press

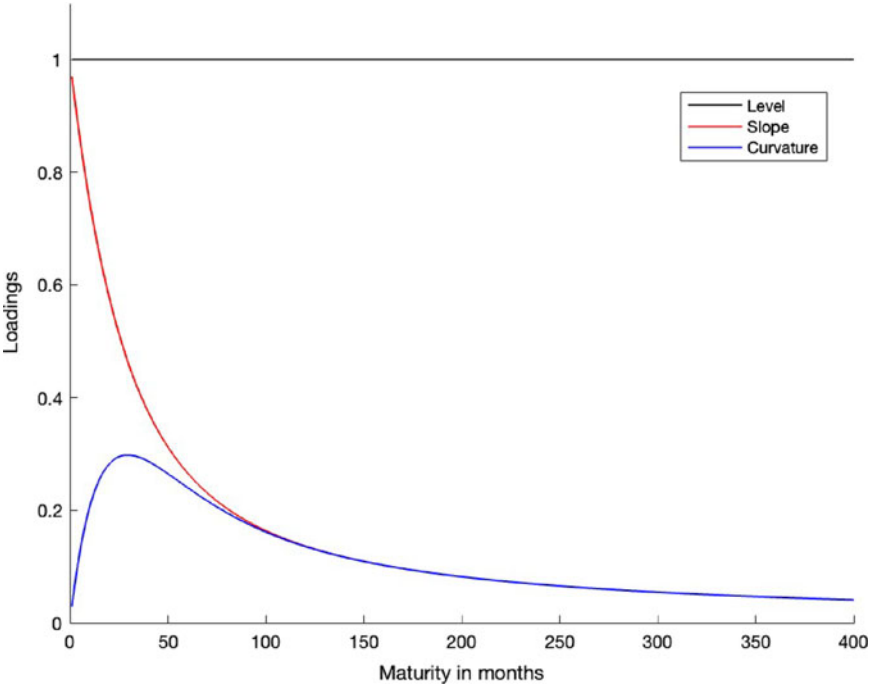


Figure 1. Factor loadings of the DNS model with $\lambda = 0.0609$.

capturing the complex dynamics of yield curves. The applications of the FDA in the interest rate market were explored in Bowsher and Meeks (2008) and Jiang (2014).

It is noteworthy that, in reality, data are often incomplete. In the presence of missing data, bootstrapping methods are commonly used to handle the gaps. Different bootstrapping methods were discussed in Ametrano and Bianchetti (2013) and Peters and Loke (n.d.). In this paper, missing data can occur in both the reference country-specific yields $Y_t^{(r)}(\tau_i)$ and the response country-specific yields $Y_t(\tau_i)$. For the former, given the small amount of missing data in our datasets, we use linear interpolation to fill in the missing values for simplicity. For the latter, we define a binary variable S_{ti} to track the missing data:

$$S_{ti} = \begin{cases} 1 & \text{if } Y_t(\tau_i) \text{ is recorded} \\ 0 & \text{otherwise.} \end{cases}$$

The extended model is given as:

$$\tilde{Y}_t(\tau_i)|Y_t^{(r)}(\cdot) = \left[F_{1,t} + F_{2,t}\left(\frac{1-e^{-\lambda\tau_i}}{\lambda\tau_i}\right) + F_{3,t}\left(\frac{1-e^{-\lambda\tau_i}}{\lambda\tau_i} - e^{-\lambda\tau_i}\right) + \int_0^{\tau_N} \gamma_i(s) Y_t^{(r)}(s)ds + \epsilon_t(\tau_i)\right] \cdot S_{ti}, \tag{12}$$

and the state equation remains unchanged:

$$F_{j,t} = \psi_{j,0} + \psi_{j,1} F_{j,t-1} + \eta_{j,t}, \quad j \in \{1, 2, 3\}. \tag{13}$$

If data are complete, this model reduces to Equations (8) and (9). Here, $Y_t^{(r)}(s)$ represents the yield curve of a reference country at time t, and $\gamma_i(s)$ are the functional coefficients. In this study, we assume that the yield curve of the response country at time t depends only on the yield curve of the

https://doi.org/10.1017/S174849952610027X Published online by Cambridge University Press

reference country at the current time t and not on previous times. Additionally, we assume that the functional coefficient $\gamma_i(s)$ is time-invariant and varies across different maturities of bonds from the response country. We refer to this model as the DNS-FR model.

However, estimating the functional coefficient $\gamma_i(s)$ is challenging. Therefore, in the next section, we will transform the functional regression component into a weighted sum of a finite number of factors.

4. Functional representation and transformation

In order to transform the integral representation of the functional regression into a vector operation suitable for linear estimation, this section introduces the kPCA method. The kPCA procedure is employed to extract a finite set of factors from the yields of the reference country. Compared with traditional PCA, kPCA offers a key advantage in capturing nonlinear structures within the data while effectively reducing dimensionality. A similar methodology has been applied in the modeling of green bonds in Campi *et al.* (2024). The detailed derivation of the kPCA procedure is provided in Appendix A.

Consider the bootstrapped input matrix of bond yields for the reference country:

$$\boldsymbol{Y}^{(r)}_{N\times T} = \begin{bmatrix} Y_1^{(r)}(\tau_1) & Y_2^{(r)}(\tau_1) & \cdots & Y_T^{(r)}(\tau_1) \\ Y_1^{(r)}(\tau_2) & Y_2^{(r)}(\tau_2) & \cdots & Y_T^{(r)}(\tau_2) \\ \vdots & \vdots & \ddots & \vdots \\ Y_1^{(r)}(\tau_N) & Y_2^{(r)}(\tau_N) & \cdots & Y_T^{(r)}(\tau_N) \end{bmatrix}.$$

We denote $\boldsymbol{Y}^{(r)}(\tau_i) = \left[Y_1^{(r)}(\tau_i), Y_2^{(r)}(\tau_i), \ldots, Y_T^{(r)}(\tau_i)\right]^\top$ as the time series of the yields of the bonds with maturity τ_i. Assume $\boldsymbol{\phi}: \mathcal{Y} \to \mathcal{F}$ is a nonlinear mapping from the observed input space $\mathcal{Y} \subset \mathbb{R}^T$ to the feature space $\mathcal{F} \subset \mathbb{R}^T$ such that $\boldsymbol{\phi}(\boldsymbol{Y}^{(r)}(\tau_i)) = \left[\phi_1(\boldsymbol{Y}^{(r)}(\tau_i)), \ldots, \phi_T(\boldsymbol{Y}^{(r)}(\tau_i))\right]^\top$.

Let $\boldsymbol{\Phi}$ be an $N \times T$ matrix:

$$\boldsymbol{\Phi}_{N\times T} = \begin{bmatrix} \phi_1(\boldsymbol{Y}^{(r)}(\tau_1)) & \cdots & \phi_T(\boldsymbol{Y}^{(r)}(\tau_1)) \\ \vdots & \ddots & \vdots \\ \phi_1(\boldsymbol{Y}^{(r)}(\tau_N)) & \cdots & \phi_T(\boldsymbol{Y}^{(r)}(\tau_N)) \end{bmatrix}.$$

The objective of kPCA is to find a linear projection that projects $\boldsymbol{\Phi}$ onto uncorrelated components denoted $\boldsymbol{A}$, with lower dimensionality. Each point $\boldsymbol{\phi}(\boldsymbol{Y}^{(r)}(\tau_i))$ can be expressed as a linear combination of $Q \leq T$ vectors of dimension T:

$$\boldsymbol{\phi}(\boldsymbol{Y}^{(r)}(\tau_i)) = \sum_{q=1}^{Q} \alpha_{i,q} \boldsymbol{v}_q,$$

where $\boldsymbol{v}_q$ are orthonormal basis vectors, and the coefficient vectors $\boldsymbol{\alpha}_q = [\alpha_{1,q}, \ldots, \alpha_{N,q}]^\top$ satisfy

$$\boldsymbol{\alpha}_q^\top \boldsymbol{\alpha}_q = \sum_{i=1}^{N} \alpha_{i,q}^2 = \lambda_q,$$

with λ_q being the qth eigenvalue of $\boldsymbol{\Phi}^\top \boldsymbol{\Phi}$.

In practice, the explicit form of the mapping $\boldsymbol{\phi}(\cdot)$ is typically unknown, and thus λ_q and $\boldsymbol{v}_q$ cannot be computed directly. To address this, we introduce a kernel function $k: \mathcal{Y} \times \mathcal{Y} \to \mathcal{F}$,

https://doi.org/10.1017/S174849952610027X Published online by Cambridge University Press

which defines the inner product in the feature space $\mathcal{F}$:

$$k(\boldsymbol{Y}^{(r)}(\tau_i), \boldsymbol{Y}^{(r)}(\tau_j)) = \boldsymbol{\Phi}(\boldsymbol{Y}^{(r)}(\tau_i))^\top \boldsymbol{\Phi}(\boldsymbol{Y}^{(r)}(\tau_j)) = \sum_{k=1}^{T} \phi_k(\boldsymbol{Y}^{(r)}(\tau_i))\phi_k(\boldsymbol{Y}^{(r)}(\tau_j)) \tag{14}$$

for $i, j \in \{1, \ldots, N\}$. Using standard matrix algebra, the eigenvectors can then be expressed as

$$\boldsymbol{v}_q^\top = \sum_{i=1}^{N} w_{i,q} \boldsymbol{\Phi}(\boldsymbol{Y}^{(r)}(\tau_i)),$$

and the principal component is given by

$$\alpha_{m,q} = \sum_{i=1}^{N} w_{i,q} k(\boldsymbol{Y}^{(r)}(\tau_m), \boldsymbol{Y}^{(r)}(\tau_i)), \tag{15}$$

where $w_{i,q}$ denotes the weights. For a new sample $\boldsymbol{Y}(\tau^*)$, where $\tau^* \notin \{\tau_1, \ldots, \tau_N\}$ and $\tau^* \in [0, \tau_{max}]$, the projection onto the qth component is

$$\alpha_{*,q} = \sum_{i=1}^{N} w_{i,q} k(\boldsymbol{Y}(\tau^*), \boldsymbol{Y}(\tau_i)). \tag{16}$$

In this paper, we choose the radial basis function (RBF) kernel, which is of the form

$$k(\boldsymbol{x}, \boldsymbol{Y}) = \exp\left(-\iota ||\boldsymbol{x} - \boldsymbol{Y}||^2\right), \tag{17}$$

where $\iota > 0$ is the hyperparameter. We will discuss the estimation of ι in Section 5.1. The validation of the RBF kernel is proved in Shawe-Taylor and Cristianini (2004). Here, we choose the RBF kernel because it is both universal (Wang et al., 2004; Ismayilova & Ismayilov, 2024) and characteristic (Sriperumbudur et al., 2011; Szabó & Sriperumbudur, 2018). A universal kernel means that it can approximate any continuous function on a compact domain, while a characteristic kernel ensures that it uniquely distinguishes probability distributions. Other popular kernel function options include the polynomial kernel, Square Bessel kernel, graph kernel, and ANOVA kernel, though these other kernel choices, whilst widely used, are typically not provably characteristic and universal.

The standard approach to learning hyperparameters of the kernel in such a regression setting is via either maximum likelihood procedures or cross-validation methods. In this work, we adopted a nonlinear maximum likelihood procedure, with a simple and reliable 2-dimensional grid search procedure. Details are available in the GitHub repository accompanying this manuscript.[1]

Subsequently, the functional regression term in Equation (8) is expressed as a weighted sum of a finite number of factors by applying the Karhunen-Loeve theorem:

Theorem 1 (Karhunen-Loeve theorem). *Suppose X_t is a zero-mean stochastic process for $t \in [a, b]$. $K(s, t)$ is the continuous covariance function. Then X_t can be expressed as*

$$X_t = \sum_{j=1}^{\infty} Z_j e_j(t),$$

where $Z_j = \int_a^b X_t e_j(t) dt$ and $e_j(t)$ are orthonormal basis functions defined in (18).

The orthonormal functions are defined as follows:

Definition 1. *Two real-valued functions $f(x)$ and $g(x)$ are orthonormal over the interval $[a, b]$ if*

[1] Github: https://github.com/peilun-he/State-Space-Dynamic-Functional-Regression-for-Multicurve.

https://doi.org/10.1017/S174849952610027X Published online by Cambridge University Press

1. $\int_a^b f(x)g(x)dx = 0$
2. $||f(x)||_2 = ||g(x)||_2 = \left[\int_a^b |f(x)|^2 dx\right]^{1/2} = \left[\int_a^b |g(x)|^2 dx\right]^{1/2} = 1$

In this paper, we choose $e_q(\tau_i) = \alpha_{i,q}\boldsymbol{v}_q$[2] as the orthogonal basis functions, so that $\boldsymbol{\Phi}(\boldsymbol{Y}^{(r)}(\tau_i)) = \sum_{q=1}^{Q} e_q(\tau_i)$. Therefore, we have

$$e_q(\tau_i) = \alpha_{i,q}\boldsymbol{v}_q = \sum_{j=1}^{N} w_{j,q} k(\boldsymbol{Y}^{(r)}(\tau_i), \boldsymbol{Y}^{(r)}(\tau_j))\boldsymbol{v}_q. \tag{18}$$

Using the Karhunen-Loeve theorem, we express $Y_t^{(r)}(s)$ and $\gamma_i(s)$ as follows:

$$Y_t^{(r)}(s) = \sum_{j=1}^{\infty} U_{tj} e_j(s) \tag{19}$$

and

$$\gamma_i(s) = \sum_{k=1}^{\infty} \gamma_{i,k} e_k(s), \tag{20}$$

where $U_{tj} = \int_0^{\tau_N} Y_t^{(r)}(s)e_j(s)ds$ and $\gamma_{i,k} = \int_0^{\tau_N} \gamma_i(s)e_k(s)ds$. We then have:

$$\begin{aligned}
\int_0^{\tau_N} \gamma_i(s) Y_t^{(r)}(s)ds &= \int_0^{\tau_N} \left(\sum_{k=1}^{\infty} \gamma_{i,k} e_k(s)\right)\left(\sum_{j=1}^{\infty} U_{tj} e_j(s)\right) ds \\
&= \sum_{j=k,j=1}^{\infty} \gamma_{i,j} U_{tj} \int_0^{\tau_N} \left(e_j(s)\right)^2 ds + \sum_{j\neq k} \gamma_{i,k} U_{tj} \int_0^{\tau_N} e_k(s)e_j(s)ds \\
&= \sum_{j=1}^{\infty} \gamma_{i,j} U_{tj} \approx \sum_{j=1}^{Q} \gamma_{i,j} U_{tj}.
\end{aligned} \tag{21}$$

Thus, the DNS-FR model given in Equations (8) and (9) can be rewritten as:

$$Y_t(\tau_i) = F_{1,t} + F_{2,t}\left(\frac{1-e^{-\lambda\tau_i}}{\lambda\tau_i}\right) + F_{3,t}\left(\frac{1-e^{-\lambda\tau_i}}{\lambda\tau_i} - e^{-\lambda\tau_i}\right) + \sum_{j=1}^{Q} \gamma_{i,j} U_{tj} + \epsilon_t(\tau_i), \tag{22}$$

$$F_{j,t} = \psi_{j,0} + \psi_{j,1} F_{j,t-1} + \eta_{j,t}, \;\; j \in \{1, 2, 3\}. \tag{23}$$

In matrix notation, this becomes:

$$\boldsymbol{Y}_t = \boldsymbol{\Lambda}\boldsymbol{F}_t + \boldsymbol{\Gamma}\boldsymbol{U}_t + \boldsymbol{\epsilon}_t, \;\; \boldsymbol{\epsilon}_t \sim N(0, \boldsymbol{\Sigma}_\epsilon), \tag{24}$$

$$\boldsymbol{F}_t = \boldsymbol{\Psi}_0 + \boldsymbol{\Psi}_1 \boldsymbol{F}_{t-1} + \boldsymbol{\eta}_t, \;\; \boldsymbol{\eta}_t \sim N(0, \boldsymbol{\Sigma}_\eta). \tag{25}$$

Given the assumptions that the $F_{j,t}$ are uncorrelated, we have:

$$\boldsymbol{\Sigma}_\eta = \begin{bmatrix} \sigma_{\eta_1}^2 & 0 & 0 \\ 0 & \sigma_{\eta_2}^2 & 0 \\ 0 & 0 & \sigma_{\eta_3}^2 \end{bmatrix}.$$

[2]In reality, we do not know the eigenvectors $\boldsymbol{v}_q$. Therefore, we choose the eigenvectors of K as a proxy. This will guarantee the orthogonality of the basis functions.

https://doi.org/10.1017/S174849952610027X Published online by Cambridge University Press

However, $\mathbf{\Sigma}_\epsilon$ is not, generally, a diagonal matrix. That is because in the bond market, different bonds with different maturities are usually correlated to each other. Therefore, in this paper, we will consider the following three structures for $\mathbf{\Sigma}_\epsilon$, for both the DNS model and the DNS-FR model:

1. $\mathbf{\Sigma}_\epsilon$ is diagonal, and bonds with different maturities have different variances:

$$\mathbf{\Sigma}_\epsilon = \begin{bmatrix} \sigma_{\epsilon_1}^2 & 0 & \cdots & 0 \\ 0 & \sigma_{\epsilon_2}^2 & \cdots & 0 \\ \vdots & \vdots & \ddots & \vdots \\ 0 & 0 & \cdots & \sigma_{\epsilon_N}^2 \end{bmatrix}.$$

2. $\mathbf{\Sigma}_\epsilon$ has a diagonal band. Each bond is only correlated to the two bonds (one with shorter maturity, and one with longer maturity) which are closest to it, but is not correlated to others. Furthermore, we assume that all pairs of two adjacent bonds have the same correlation coefficient:

$$\mathbf{\Sigma}_\epsilon = \begin{bmatrix} \sigma_{\epsilon_1}^2 & \rho\sigma_{\epsilon_1}\sigma_{\epsilon_2} & 0 & \cdots & 0 & 0 \\ \rho\sigma_{\epsilon_1}\sigma_{\epsilon_2} & \sigma_{\epsilon_2}^2 & \rho\sigma_{\epsilon_2}\sigma_{\epsilon_3} & \cdots & 0 & 0 \\ 0 & \rho\sigma_{\epsilon_2}\sigma_{\epsilon_3} & \sigma_{\epsilon_3}^2 & \cdots & 0 & 0 \\ \vdots & \vdots & \vdots & \ddots & \vdots & \\ 0 & 0 & 0 & \cdots & \sigma_{\epsilon_{N-1}}^2 & \rho\sigma_{\epsilon_{N-1}}\sigma_{\epsilon_N} \\ 0 & 0 & 0 & \cdots & \rho\sigma_{\epsilon_{N-1}}\sigma_{\epsilon_N} & \sigma_{\epsilon_N}^2 \end{bmatrix}$$

However, it should be noted that this matrix is not always positive definite for all $\rho \in [-1, 1]$. Actually, it has been shown in Johnson *et al.* (1996) that only when ρ ranges from $-\frac{1}{2}\sqrt{1+\frac{\pi^2}{1+4N^2}}$ to $\frac{1}{2}\sqrt{1+\frac{\pi^2}{1+4N^2}}$, a positive definite matrix is guaranteed. Therefore, assuming $\theta \in \mathbb{R}$ is the input parameter, we take a transformation

$$\rho = \sqrt{1+\frac{\pi^2}{1+4N^2}} \times \frac{1}{1+e^{-\theta}} - \frac{1}{2}\sqrt{1+\frac{\pi^2}{1+4N^2}} \tag{26}$$

to make sure that ρ is in the correct range.

3. $\mathbf{\Sigma}_\epsilon$ is a full covariance matrix. To avoid a very high dimensionality of parameter space, we assume that this covariance is generated by two parameters in the following form:

$$\mathbf{\Sigma}_\epsilon = \begin{bmatrix} \sigma^2 & \sigma^2\rho & \cdots & \sigma^2\rho^{N-1} \\ \sigma^2\rho & \sigma^2 & \cdots & \sigma^2\rho^{N-2} \\ \vdots & \vdots & \ddots & \vdots \\ \sigma^2\rho^{N-1} & \sigma^2\rho^{N-2} & \cdots & \sigma^2 \end{bmatrix}$$

In this case, we assume that all bonds have the same variance, and the covariance of two bonds decays as the difference in maturities increases.

In Section 8, we will compare the in-sample estimation accuracy of the models using these three covariance structures, respectively.

https://doi.org/10.1017/S174849952610027X Published online by Cambridge University Press

5. Estimation methodology

In this section, we present the estimation methods for the model. We first discuss the estimation of the hyperparameter ι of the RBF kernel function in Section 5.1. Then, in Section 5.2, we introduce the Kalman Filter to estimate the hidden factors in a standard linear state-space model. All parameters of the state-space model are estimated by maximizing the marginal likelihood function in Sections 5.3 and 5.4.

5.1 Estimation of hyperparameters for the Kernel function

The hyperparameter ι of the RBF kernel is estimated through a grid search. We choose ι from the range 0.001 to 1 with a step size of 0.001. At each grid point, the pre-image measurement error is calculated. The point on the grid with the minimum error is selected as the optimal ι.

To prevent data leakage, the hyperparameter ι and all other model parameters are estimated exclusively using in-sample observations. Out-of-sample forecasts are then generated sequentially, conditioning only on the historical information available at each forecasting point. Moreover, the factors U_{tj} are estimated using kPCA based solely on in-sample data during the in-sample estimation stage, while in the out-of-sample forecasting stage, these factors are reconstructed using both in-sample and out-of-sample data.

5.2 Kalman Filter

The Kalman Filter is used to estimate all parameters of the DNS-FR model. We start by reparameterizing Equations (24) and (25) into a standard state-space model:

$$\boldsymbol{Y}_t - \boldsymbol{\Lambda}\boldsymbol{\mu} - \boldsymbol{\Gamma}\boldsymbol{U}_t = \boldsymbol{\Lambda}(\boldsymbol{F}_t - \boldsymbol{\mu}) + \boldsymbol{B}\boldsymbol{v}_t, \tag{27}$$

$$\boldsymbol{F}_t - \boldsymbol{\mu} = \boldsymbol{\Psi}_1(\boldsymbol{F}_{t-1} - \boldsymbol{\mu}) + \boldsymbol{D}\boldsymbol{w}_t, \tag{28}$$

where $\boldsymbol{\mu}$ is the mean vector of the hidden state vector such that $\boldsymbol{\mu} - \boldsymbol{\Psi}_1\boldsymbol{\mu} = \boldsymbol{\Psi}_0$, and $\boldsymbol{B}$ and $\boldsymbol{D}$ are Cholesky decomposition of $\boldsymbol{\Sigma}_\epsilon$ and $\boldsymbol{\Sigma}_\eta$, respectively. $\boldsymbol{v}_t$ and $\boldsymbol{w}_t$ are uncorrelated unit-variance white noise processes. We define $\boldsymbol{Z}_t := \boldsymbol{Y}_t - \boldsymbol{\Lambda}\boldsymbol{\mu} - \boldsymbol{\Gamma}\boldsymbol{U}_t$ and $\boldsymbol{X}_t := \boldsymbol{F}_t - \boldsymbol{\mu}$ representing the measurement and state vectors. Therefore, Equations (27) and (28) can be rewritten as:

$$\boldsymbol{Z}_t = \boldsymbol{\Lambda}\boldsymbol{X}_t + \boldsymbol{B}\boldsymbol{v}_t, \tag{29}$$

$$\boldsymbol{X}_t = \boldsymbol{\Psi}_1\boldsymbol{X}_{t-1} + \boldsymbol{D}\boldsymbol{w}_t. \tag{30}$$

For the DNS model, we have similar notations but $\boldsymbol{\Gamma}\boldsymbol{U}_t = 0$.

Moreover, we use the following notations to represent the expectation and covariance matrix of the state vector $\boldsymbol{X}_t$:

$$\begin{aligned} \boldsymbol{a}_{t|t-1} &:= \mathbb{E}(\boldsymbol{X}_t|\boldsymbol{Z}_{1:t-1}), & \boldsymbol{P}_{t|t-1} &:= Cov(\boldsymbol{X}_t|\boldsymbol{Z}_{1:t-1}), \\ \boldsymbol{a}_t &:= \mathbb{E}(\boldsymbol{X}_t|\boldsymbol{Z}_{1:t}), & \boldsymbol{P}_t &:= Cov(\boldsymbol{X}_t|\boldsymbol{Z}_{1:t}) \end{aligned}$$

$\boldsymbol{Z}_{1:t}$ represents all vectors $\boldsymbol{Z}_1, \boldsymbol{Z}_2, \ldots, \boldsymbol{Z}_t$. We assume that $\boldsymbol{X}_t$ is a Markov process, so that the distribution at time t depends only on the state in the previous time $t-1$.

Now, we present the algorithm of the Kalman Filter. The system starts from an initial state $\boldsymbol{X}_0 \sim N(\boldsymbol{a}_0, \boldsymbol{P}_0)$, and all point estimates $\boldsymbol{a}_t$ and covariance $\boldsymbol{P}_t$ are calculated recursively in a two-stage process involving a prediction stage and a update stage.

First, given observations $\boldsymbol{Z}_{1:t-1}$ and state $\boldsymbol{X}_{t-1}$, the prediction of the distribution of $\boldsymbol{X}_t$ is calculated by

$$f(\boldsymbol{X}_t|\boldsymbol{Z}_{1:t-1}) = \int f(\boldsymbol{X}_t|\boldsymbol{X}_{t-1}, \boldsymbol{Z}_{1:t-1}) f(\boldsymbol{X}_{t-1}|\boldsymbol{Z}_{1:t-1}) d\boldsymbol{X}_{t-1}, \tag{31}$$

https://doi.org/10.1017/S174849952610027X Published online by Cambridge University Press

where $f(\cdot)$ represents the density function. As $\boldsymbol{X}_t|\boldsymbol{X}_{t-1}, \boldsymbol{Z}_{1:t-1} \sim N(\boldsymbol{\Psi}_1\boldsymbol{X}_{t-1}, \boldsymbol{\Sigma}_\eta)$ and $\boldsymbol{X}_{t-1}|\boldsymbol{Z}_{1:t-1} \sim N(\boldsymbol{a}_{t-1}, \boldsymbol{P}_{t-1})$, we have $\boldsymbol{X}_t|\boldsymbol{Z}_{1:t-1} \sim N(\boldsymbol{\Psi}_1\boldsymbol{a}_{t-1}, \boldsymbol{\Psi}_1\boldsymbol{P}_{t-1}\boldsymbol{\Psi}_1^\top + \boldsymbol{\Sigma}_\eta)$. The point estimates and the covariance matrix are

$$\boldsymbol{a}_{t|t-1} = \boldsymbol{\Psi}_1\boldsymbol{a}_{t-1} \tag{32}$$

and

$$\boldsymbol{P}_{t|t-1} = \boldsymbol{\Psi}_1\boldsymbol{P}_{t-1}\boldsymbol{\Psi}_1^\top + \boldsymbol{\Sigma}_\eta. \tag{33}$$

Next, when a new observation $\boldsymbol{Z}_t$ is available, we update the distribution as

$$f(\boldsymbol{X}_t|\boldsymbol{Z}_{1:t}) \propto f(\boldsymbol{Z}_t|\boldsymbol{X}_t, \boldsymbol{Z}_{1:t-1}) f(\boldsymbol{X}_t|\boldsymbol{Z}_{1:t-1}), \tag{34}$$

which is a direct result of Bayes' Theorem. From the measurement equation, we have $\boldsymbol{Z}_t|\boldsymbol{X}_t, \boldsymbol{Z}_{1:t-1} \sim N(\boldsymbol{\Lambda}\boldsymbol{X}_t, \boldsymbol{\Sigma}_\epsilon)$. Then, using some basic properties of normal distribution, we have $\boldsymbol{X}_t|\boldsymbol{Z}_{1:t} \sim N(\boldsymbol{a}_{t|t-1} + \boldsymbol{K}_t(\boldsymbol{Z}_t - \boldsymbol{\Lambda}\boldsymbol{a}_{t|t-1}), (\boldsymbol{I} - \boldsymbol{K}_t\boldsymbol{\Lambda})\boldsymbol{P}_{t|t-1})$, where $\boldsymbol{I}$ is the identity matrix, and $\boldsymbol{K}_t = \boldsymbol{P}_{t|t-1}\boldsymbol{\Lambda}^\top(\boldsymbol{\Lambda}\boldsymbol{P}_{t|t-1}\boldsymbol{\Lambda}^\top + \boldsymbol{\Sigma}_\epsilon)^{-1}$ is the Kalman gain matrix. The updated point estimates and covariance matrix are

$$\boldsymbol{a}_t = \boldsymbol{a}_{t|t-1} + \boldsymbol{K}_t(\boldsymbol{Z}_t - \boldsymbol{\Lambda}\boldsymbol{a}_{t|t-1}) \tag{35}$$

and

$$\boldsymbol{P}_t = (\boldsymbol{I} - \boldsymbol{K}_t\boldsymbol{\Lambda})\boldsymbol{P}_{t|t-1}. \tag{36}$$

Finally, we repeat all the steps for $t \in \{1, \ldots, N\}$.

5.3 Maximum marginal likelihood estimation

In this section, we discuss the method for estimating unknown parameters, denoted by θ, by maximizing the marginal likelihood.

The marginal distribution of $\boldsymbol{Z}_t|\boldsymbol{Z}_{1:t-1}$ is given by

$$f(\boldsymbol{Z}_t|\boldsymbol{Z}_{1:t-1}) = \int f(\boldsymbol{Z}_t|\boldsymbol{X}_t, \boldsymbol{Z}_{1:t-1}) f(\boldsymbol{X}_t|\boldsymbol{Z}_{1:t-1}) d\boldsymbol{X}_t. \tag{37}$$

From the previous section, we know that $\boldsymbol{Z}_t|\boldsymbol{X}_t, \boldsymbol{Z}_{1:t-1} \sim N(\boldsymbol{\Lambda}\boldsymbol{X}_t, \boldsymbol{\Sigma}_\epsilon)$ and $\boldsymbol{X}_t|\boldsymbol{Z}_{1:t-1} \sim N(\boldsymbol{a}_{t|t-1}, \boldsymbol{P}_{t|t-1})$. Therefore, we have $\boldsymbol{Z}_t|\boldsymbol{Z}_{1:t-1} \sim N(\boldsymbol{\Lambda}\boldsymbol{a}_{t|t-1}, \boldsymbol{\Lambda}\boldsymbol{P}_{t|t-1}\boldsymbol{\Lambda}^\top + \boldsymbol{\Sigma}_\epsilon)$. Moreover, we define the estimation error of $\boldsymbol{Z}_t$ as

$$\boldsymbol{e}_t = \boldsymbol{Z}_t - \hat{\boldsymbol{Z}}_t = \boldsymbol{Z}_t - \boldsymbol{\Lambda}\boldsymbol{a}_{t|t-1} \tag{38}$$

and the covariance matrix is

$$\boldsymbol{L}_{t|t-1} = Cov(\boldsymbol{e}_t|\boldsymbol{Z}_{1:t-1}) = Cov(\boldsymbol{Z}_t|\boldsymbol{Z}_{1:t-1}) = \boldsymbol{\Lambda}\boldsymbol{P}_{t|t-1}\boldsymbol{\Lambda}^\top + \boldsymbol{\Sigma}_\epsilon. \tag{39}$$

Ignoring the constant terms, the log-likelihood function is given by

$$l(\theta; \boldsymbol{Z}_{1:N}) = -\frac{1}{2}\sum_{t=1}^{N}\left(\boldsymbol{e}_t^\top \boldsymbol{L}_{t|t-1}^{-1}\boldsymbol{e}_t + \log|\boldsymbol{L}_{t|t-1}|\right). \tag{40}$$

The maximum likelihood estimation (MLE) $\hat{\theta}$ maximizes the Equation (40).

5.4 Overfitting and regularization

The DNS-FR models in Equations (22) and (23) may be subject to overfitting, particularly due to the inclusion of functional components. To address this issue, regularization techniques such as ridge and lasso regression can be applied.

https://doi.org/10.1017/S174849952610027X Published online by Cambridge University Press

A practical approach involves first estimating the baseline DNS model given by Equations (10) and (11) to obtain the residuals $\hat{\hat{\epsilon}}_t(\tau_i)$. The functional component is then fitted to these residuals using a penalized regression of the form:

$$\hat{\hat{\epsilon}}_t(\tau_i) = \sum_{j=1}^{Q} \gamma_{i,j} U_{tj} + e_t(\tau_i).$$

The lasso and ridge estimators are obtained by minimizing the following penalized loss functions:

$$\text{Lasso: } \sum_{t=1}^{T} \left(\hat{\hat{\epsilon}}_t(\tau_i) - \sum_{j=1}^{Q} \gamma_{i,j} U_{tj} \right)^2 + \kappa \sum_{j=1}^{Q} |\gamma_{i,j}|,$$

$$\text{Ridge: } \sum_{t=1}^{T} \left(\hat{\hat{\epsilon}}_t(\tau_i) - \sum_{j=1}^{Q} \gamma_{i,j} U_{tj} \right)^2 + \kappa \sum_{j=1}^{Q} \gamma_{i,j}^2,$$

where $\kappa > 0$ is the tuning parameter that controls the strength of the penalty term.

6. Forecasting methodology

In this section, we discuss the procedures for forecasting the response country's yields over a h-month horizon. First, we discuss the prediction of the measurement $\boldsymbol{Z}_{N+1:N+h}$. We start with the 1-step ahead forecasting and extend to h-step ahead forecasting.

The conditional density of the measurement is

$$f(\boldsymbol{Z}_{N+1}|\boldsymbol{Z}_{1:N}) = \int f(\boldsymbol{Z}_{N+1}|\boldsymbol{X}_{N+1}, \boldsymbol{Z}_{1:N}) f(\boldsymbol{X}_{N+1}|\boldsymbol{Z}_{1:N}) d\boldsymbol{X}_{N+1}. \tag{41}$$

Using the results of Section 5.3, we have $\boldsymbol{Z}_{N+1}|\boldsymbol{Z}_{1:N} \sim N(\boldsymbol{\Lambda}\boldsymbol{a}_{N+1|N}, \boldsymbol{L}_{N+1|N})$. So, our prediction is

$$\hat{\boldsymbol{Z}}_{N+1}|Z_{1:N} = \boldsymbol{\Lambda}\boldsymbol{a}_{N+1|N} = \boldsymbol{\Lambda}\boldsymbol{\Psi}_1\boldsymbol{a}_N. \tag{42}$$

Then, for a h-step ahead forecasting, we can consider it as a sequence of 1-step ahead forecasting. The conditional density is given by

$$f(\boldsymbol{Z}_{N+h}|\boldsymbol{Z}_{1:N}, \hat{\boldsymbol{Z}}_{N+1:N+h-1}) = \int f(\boldsymbol{Z}_{N+h}|\boldsymbol{X}_{N+h}, \boldsymbol{Z}_{1:N}, \hat{\boldsymbol{Z}}_{N+1:N+h-1}) f(\boldsymbol{X}_{N+h}|\boldsymbol{Z}_{1:N}, \hat{\boldsymbol{Z}}_{N+1:N+h-1}) d\boldsymbol{X}_{N+h}. \tag{43}$$

Using a similar method, we have $\boldsymbol{Z}_{N+h}|\boldsymbol{Z}_{1:N}, \hat{\boldsymbol{Z}}_{N+1:N+h-1} \sim N(\boldsymbol{\Lambda}\boldsymbol{a}_{N+h|N}, \boldsymbol{L}_{N+h|N})$. As we do not have the real values for $\hat{\boldsymbol{Z}}_{N+1:N+h-1}$ but only the predicted values $\hat{\hat{\boldsymbol{Z}}}_{N+1:N+h-1}$, the prediction error $\boldsymbol{e}_i = 0$ for all $N+1 \le i \le N+h$ and therefore the point estimates of the state variable $\boldsymbol{a}_{N+h|N} = \boldsymbol{\Psi}_1\boldsymbol{a}_{N+h-1|N} = \cdots = \boldsymbol{\Psi}_1^h\boldsymbol{a}_N$. Our prediction is

$$\hat{\boldsymbol{Z}}_{N+h}|\boldsymbol{Z}_{1:N}, \hat{\boldsymbol{Z}}_{N+1:N+h-1} = \boldsymbol{\Lambda}\boldsymbol{a}_{N+h|N} = \boldsymbol{\Lambda}\boldsymbol{\Psi}_1^h\boldsymbol{a}_N. \tag{44}$$

The corresponding covariance matrix is

$$\boldsymbol{L}_{N+h|N} := Cov(\boldsymbol{Z}_{N+h}|\boldsymbol{Z}_{1:N}) = Cov(\boldsymbol{Y}_{N+h}|\boldsymbol{Y}_{1:N}, \boldsymbol{U}_{1:N}) = \boldsymbol{\Lambda} Cov(\boldsymbol{X}_{N+h}|\boldsymbol{Z}_{1:N})\boldsymbol{\Lambda} + \boldsymbol{\Sigma}_\epsilon, \tag{45}$$

where

$$Cov(\boldsymbol{X}_{N+h}|\boldsymbol{Z}_{1:N}) = \boldsymbol{\Psi}_1 Cov(\boldsymbol{X}_{N+h-1}|\boldsymbol{Z}_{1:N})\boldsymbol{\Psi}_1^\top + \boldsymbol{\Sigma}_\eta \tag{46}$$

is calculated recursively.

https://doi.org/10.1017/S174849952610027X Published online by Cambridge University Press

Now, we discuss the prediction of the response country's yields. We divide the forecasting into the following three steps:

1. Forecast the US yields $\hat{\boldsymbol{Y}}^{(r)}_{N+1}, \hat{\boldsymbol{Y}}^{(r)}_{N+2}, \ldots, \hat{\boldsymbol{Y}}^{(r)}_{N+h}$ over the horizon h using the DNS model by Equation (44), where $\hat{\boldsymbol{Z}}_{N+i} = \hat{\boldsymbol{Y}}^{(r)}_{N+i} - \boldsymbol{\Lambda}\boldsymbol{\mu}$.
2. Reconstruct factors $\hat{\boldsymbol{U}}_1, \ldots, \hat{\boldsymbol{U}}_{N+h}$ using both in-sample data $\boldsymbol{Y}^{(r)}_1, \ldots, \boldsymbol{Y}^{(r)}_t$ and predicted data $\hat{\boldsymbol{Y}}^{(r)}_{N+1}, \ldots, \hat{\boldsymbol{Y}}^{(r)}_{N+h}$ through kPCA. Keep the hyperparameter constant.
3. Forecast the response country's yields $\hat{\boldsymbol{Y}}_{N+1}, \ldots, \hat{\boldsymbol{Y}}_{N+h}$ by Equation (44) using DNS-FR model, where $\hat{\boldsymbol{Z}}_{N+i} = \hat{\boldsymbol{Y}}_{N+i} - \boldsymbol{\Lambda}\boldsymbol{\mu} - \boldsymbol{\Gamma}\hat{\boldsymbol{U}}_{N+i}$. The covariance matrix is given in Equation (45) as the terms $\boldsymbol{\Lambda}\boldsymbol{\mu}$ and $\boldsymbol{\Gamma}\hat{\boldsymbol{U}}_{N+i}$ are constants.

In step 2, both in-sample data and predicted data are used for two reasons. First, the forecast horizon is not too long compared to the in-sample horizon. If only predicted data are used, the extracted factors may not be accurate. Second, incorporating the true trajectories into the reconstruction produces a more stable representation.

7. Data

In this paper, we focus on examining the relative spreads of seven countries/regions (the UK, Germany, France, Italy, Japan, Australia, and the European Union) with respect to US bond yields, which serve as the reference yield. The data used in this analysis consist of monthly data from January 2010 to December 2020.[3] We use the first ten years as in-sample data to estimate unknown parameters and hidden state variables, and the data for the last year for out-of-sample forecasting.

The original data contain the following maturities:

- United States (US): with maturities 1, 3, 6 months, and 1, 2, 3, 5, 7, 10, and 30 years.
- United Kingdom (UK): with maturities 1, 3, 6 months, 1, 2, 3, 5, 10, 20, and 30 years.
- Germany (DE): with maturities 3, 6, 9 months, and 1, 2, 3, 5, 10, 20, and 30 years.
- France (FR): with maturities 1, 3, 6, 9 months, and 2, 3, 5, 10, 20, and 30 years.
- Italy (IT): with maturities 6, 9 months, and 2, 3, 5, 10, and 30 years.
- Japan (JP): with maturities 6 months, and 1, 2, 3, 5, 10, 20, and 30 years.
- Australia (AU): with maturities 1, 2, 3, 5, and 10 years.
- European Union (EU): with maturities 1, 3, 6, 9 months, 1, 2, 3, 5, 7, 10, 20, and 30 years.

To provide a better interpretation, we match each country's maturities to 1, 3, 6, 9 months, 1, 2, 3, 5, 7, 10, 20, and 30 years. For countries/regions without all these maturities, we estimated the missing maturities using the static Nelson–Siegel model:

$$Y_t(\tau_i) = F_{1,t} + F_{2,t}\left(\frac{1 - e^{-\lambda\tau_i}}{\lambda\tau_i}\right) + F_{3,t}\left(\frac{1 - e^{-\lambda\tau_i}}{\lambda\tau_i} - e^{-\lambda\tau_i}\right) + \nu_t(\tau_i), \tag{47}$$

where $F_{1,t}$, $F_{2,t}$, and $F_{3,t}$ are hidden factors representing the level, slope, and curvature. The difference between Equation (47) and the DNS model described in Section 3.1 is that for Equation (47), we do not assume any dynamics of the factors $F_{i,t}$, for $i \in \{1, 2, 3\}$. Instead, they are estimated day by day using the least squares method. Figure 2 shows the UK yield curves for the original data and the data after maturity matching, respectively. The 9-month and 7-year bond yields are interpolated in the right sub-figure. Additionally, all missing values are replaced by interpolated values.

[3]Data were obtained from https://www.tradingview.com/.

https://doi.org/10.1017/S174849952610027X Published online by Cambridge University Press

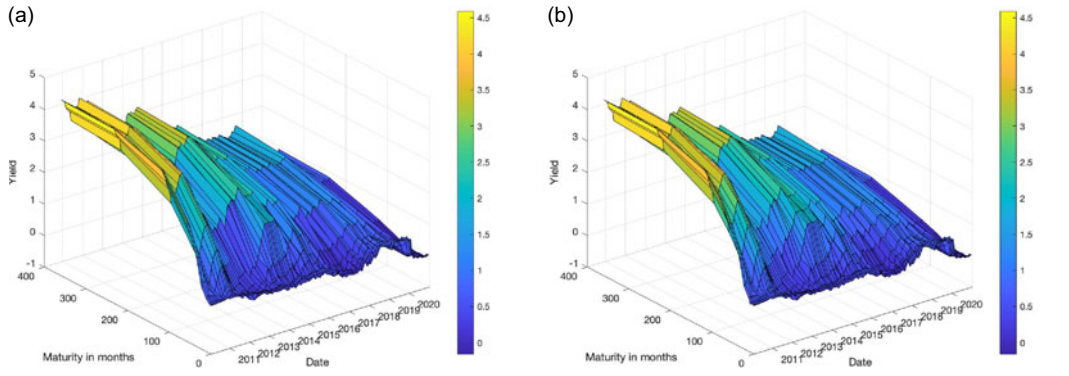


Figure 2. UK yield curves from January 2010 to December 2020. The left figure is for the original data, and the right figure is for the data after maturity matching. 9-month yield and 7-year (84-month) yield are interpolated in the right figure.

8. Empirical analysis

In this section, we present the empirical results. We first show the in-sample estimations using the DNS model and the DNS-FR model in Sections 8.1 and 8.2, respectively. Section 8.3 gives the out-of-sample forecasting. To assess the potential issue of overfitting, we compare the functional regression model with a simple addition model in Section 8.4. Then, we test the performance of the DNS-FR model under a permanent shock and a temporary shock in Section 8.5. Finally, one application of the DNS-FR model in the construction of a bond ladder portfolio for risk management is given in Section 8.6.

8.1 Dynamic Nelson–Siegel model

We first present the estimation results of the DNS model, which serves as a benchmark. Model parameters and hidden state variables are jointly estimated by maximizing the marginal likelihood function described in Section 5.3. In this paper, λ is fixed at 0.0609, as in Diebold and Li (2006).

The in-sample Root Mean Squared Error (RMSE) using covariance structure 2 is provided in Table 1. The in-sample RMSE for the DNS model using covariance structures 1 and 3 is given in Appendix B. We first discuss the differences between these covariance structures, as outlined in Section 4. Overall, the differences in mean RMSE are minimal. For long-end maturities, specifically 20-year and 30-year maturities, covariance structure 3 provides the most accurate estimation. However, for short-end and middle maturities, covariance structure 3 exhibits the highest RMSE. It also has the highest mean RMSE for most countries/regions, except Japan. Therefore, covariance structure 3 is not the best choice for this study. Covariance structures 1 and 2 are more evenly matched, with structure 2 outperforming structure 1 for some countries/regions and vice versa. Considering that covariance structure 2 shows some dependencies between yields with different maturities, which is more realistic in the bond market, while structure 1 assumes all yields are uncorrelated, we choose to use structure 2 for further analysis.

Focusing on covariance structure 2, most countries/regions exhibit a high RMSE for long-end maturities, with the exception of Italy. Italy has a low RMSE for long-end maturities but a high RMSE for middle maturities, between 3 years and 10 years. Similar patterns are observed for the UK, France, and the European Union, which also show high RMSEs for middle maturities. Conversely, the DNS model fits the short-end maturities well across all countries/regions.

These results suggest that while the DNS model generally captures the dynamics well for short-end maturities, it struggles with accuracy at longer maturities for most countries/regions.

https://doi.org/10.1017/S174849952610027X Published online by Cambridge University Press

Table 1. In-sample RMSE for DNS model using covariance structure 2

Maturity	UK	FR	IT	DE	JP	AU	EU	US
1 month	0.1313	0.1139	0.0288	0.0047	2.26e-05	0.0048	0.1984	0.0645
3 months	0.0212	0.0755	0.0007	0.0571	3.20e-15	0.0005	0.1307	0.0126
6 months	0.1027	0.0449	0.0679	0.0677	0.0323	0.0026	0.0492	0.0688
9 months	0.0511	0.0738	0.0722	0.0891	0.0071	0.0012	0.0590	0.0324
1 year	0.0999	0.0142	3.64e-13	0.1009	0.0160	0.0106	0.0867	0.0752
2 years	0.0102	0.0725	0.1096	0.0210	0.0144	0.0272	0.0145	0.0179
3 years	0.1223	0.1770	0.2409	0.1216	0.0195	0.0589	0.1305	0.1082
5 years	0.2390	0.2764	0.3754	0.1658	0.0268	0.0217	0.2097	0.1263
7 years	0.1563	0.2023	0.3206	0.0950	0.1574	0.0957	0.2067	0.0787
10 years	0.1374	0.1716	0.2214	0.1607	0.3325	0.2469	0.0904	0.1598
20 years	0.4039	0.3410	0.0532	0.4377	0.9466	0.6271	0.2843	0.3872
30 years	0.4706	0.4769	0.1233	0.4846	1.1036	0.8269	0.3049	0.5018
Mean	0.1622	0.1700	0.1345	0.1505	0.2214	0.1603	0.1471	0.1361

This discrepancy is likely due to the higher volatility and risk associated with longer-term bonds, which are not fully captured by the DNS model.

Another notable observation is the presence of extremely small values in Tables 1 and 2, in the order of less than 1e-10. This phenomenon can be explained from two perspectives. First, as discussed in Section 7, data for some countries lack certain yield curve maturities used in the analysis. These missing maturities include 9-month and 20-year maturities for the US; 9-month and 7-year maturities for the UK; 1-month and 7-year maturities for Germany; 1-year and 7-year maturities for France; 1-month, 3-month, and 1-year, 7-year, and 20-year maturities for Italy; 1-month, 3-month, 9-month, and 7-year maturities for Japan; and 1-month, 3-month, 6-month, 9-month, and 7-year, 20-year, and 30-year maturities for Australia. These missing maturities are bootstrapped with small observation errors, leading to lower estimation errors for some of these maturities. Second, there are no constraints on the error terms in Equations (24) and (25). Due to the nature of the state-space model, a higher estimated signal-to-noise ratio results in smaller estimation errors for observations. This also explains the presence of extremely small values in some cases.

8.2 DNS-FR model

In this section, we present the estimation results of the DNS-FR model. To estimate the yields of response countries, we first extract factors from US Treasury yields using kPCA as discussed in Section 4. The estimated hyperparameter for the RBF kernel is $\iota = 0.083$. After extracting these factors, we estimate the yields using the same methodology as the DNS model.

We select 3 kPCA factors for this study. Compared to the RMSE using 2 factors, the in-sample RMSE with 3 factors shows significant improvement, particularly for UK yields. Increasing the number of factors to 4 or 5 further reduces the RMSE for most countries/regions, but the improvement is marginal. Given the substantial increase in parameter space and associated computational challenges, we determine that 3 factors strike the optimal balance. Similar to the DNS model, the choice among the three covariance structures shows minimal difference. For consistency, we use covariance structure 2 for the remainder of this paper.

Table 2 presents the in-sample RMSE for the DNS-FR model with 3 factors and covariance structure 2. The in-sample RMSE for other covariance structures and factor counts is provided in Appendix C. The DNS-FR model significantly reduces the mean RMSE compared to the DNS model across all countries/regions. Specifically, for the UK, France, Germany, and European

https://doi.org/10.1017/S174849952610027X Published online by Cambridge University Press

Table 2. In-sample RMSE for DNS-FR model with 3 factors using covariance structure 2

Maturity	UK	FR	IT	DE	JP	AU	EU
1 month	0.0585	0.0474	0.0234	3.98e-15	0.0001	0.0021	0.0911
3 months	0.0115	0.0544	0.0030	0.0458	0.0002	0.0002	0.0580
6 months	0.0447	0.0336	0.0638	0.0451	0.0156	0.0002	0.0455
9 months	0.0193	0.0404	0.0682	0.0483	0.0006	0.0034	0.0357
1 year	0.0684	0.0098	2.87e-15	0.0496	0.0145	0.0289	0.0456
2 years	5.51e-15	0.0551	0.1007	0.0032	0.0131	0.0380	1.41e-14
3 years	0.0802	0.0578	0.1536	0.0443	0.0084	0.0457	0.0424
5 years	0.1639	0.1332	0.2277	0.0915	0.0063	0.0147	0.0910
7 years	0.1059	0.0811	0.2088	0.0588	0.0403	0.0566	0.1152
10 years	0.1203	0.0830	0.1591	0.0741	0.0870	0.1473	0.0696
20 years	0.0669	0.1982	0.0426	0.1534	0.2508	0.4285	0.1042
30 years	0.0775	0.3181	0.1251	0.2709	0.3515	0.5899	0.1679
Mean	0.0681	0.0927	0.0980	0.0738	0.0657	0.1130	0.0722

Union yields, the DNS-FR model outperforms the DNS model at all maturities. For Italy yields, while the DNS model shows lower RMSE at 3-month, 1-year, and 30-year maturities, the differences are minimal. For other maturities, the DNS-FR model performs better. For Japan yields, the DNS model has a slight advantage at 1-month and 3-month maturities, whereas for Australia yields, it is more accurate at 9-month, 1-year, and 2-year maturities. Otherwise, the DNS-FR model provides superior yield estimates.

As discussed in Section 8.1, the DNS model struggles with accurately estimating the yield curve for 20-year and 30-year maturities. The DNS-FR model significantly improves this issue. For UK and European Union yields, the RMSE magnitude for long-end maturities aligns closely with other maturities. The DNS model already provides accurate long-end maturity estimates for Italian yields, so the DNS-FR model does not offer much improvement here. For France, Germany, Japan, and Australia yields, the RMSE for long-end maturities remains high, but the DNS-FR model still achieves significant reductions.

For the remainder of this paper, we focus on UK yields, as the DNS-FR model performs well for both short and long maturities.

We close this subsection by discussing the structure of the yield curve. Typically, in the bond market, the yield curve is in an upward-sloping or normal shape, where short-term interest rates are lower than long-term rates due to the higher risk associated with long-term debt. However, under certain conditions, this relationship can invert, leading to an inverted yield curve where long-term bonds have lower yields than short-term bonds. Such inversions are relatively rare and noteworthy as it often indicates an unusual economic environment. Therefore, it is essential to test if models can accurately estimate yield curves in both normal and inverted configurations.

Figure 3 illustrates the estimated UK yield curves by the DNS and DNS-FR models for January 2011, August 2015, and September 2019. In January 2011, the yield curve displayed a normal upward-sloping shape. For bonds with maturities less than 120 months, both models perform similarly. However, for longer maturities, the DNS-FR model provides better estimates. In August 2015, when the curve remained in a normal shape, the DNS-FR model continued to outperform, especially for long-term bonds. Moreover, the DNS-FR model captures short-term fluctuations accurately, whereas the DNS model offers a smoothed estimation. In September 2019, the yield curve exhibited an inversion for maturities less than 60 months, before reverting to a normal slope for longer maturities. The DNS-FR model again demonstrates superior performance, accurately fitting both the inverted and normal segments of the curve.

https://doi.org/10.1017/S174849952610027X Published online by Cambridge University Press

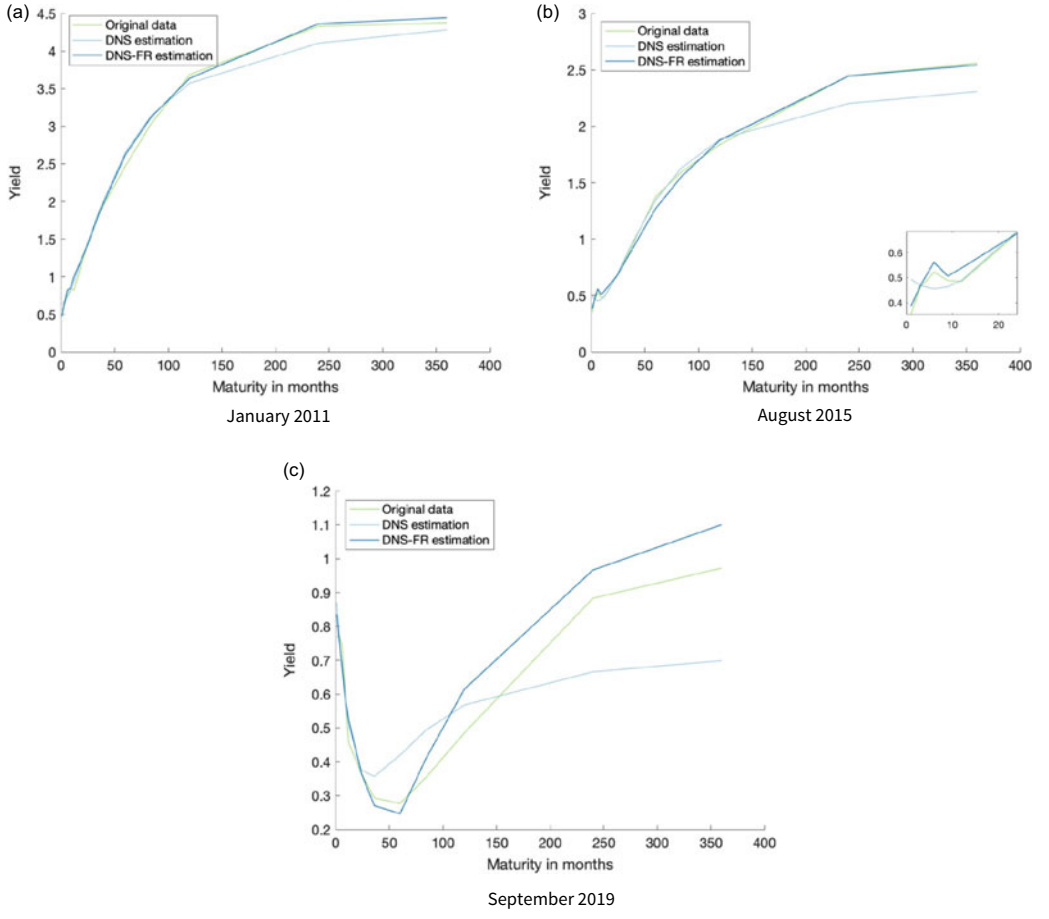


Figure 3. Estimated UK yield curves by DNS model and DNS-FR model for three different months.

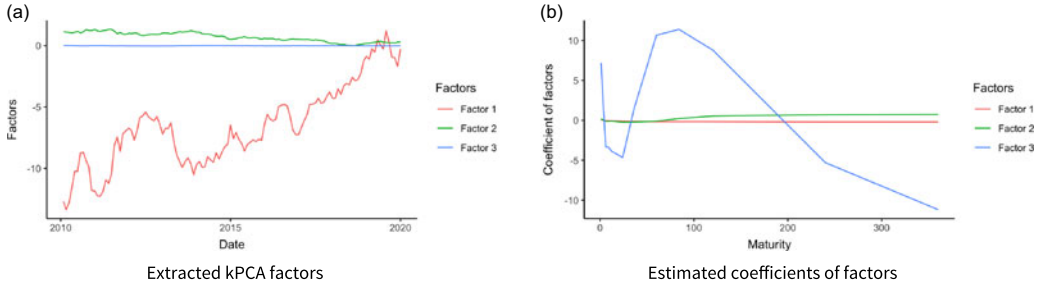


Figure 4. Extracted kPCA factors and the corresponding coefficients.

Figure 4 presents the extracted kPCA factors U_{tj} (left) and their corresponding coefficients $\gamma_{i,j}$ in Equation (22).

8.3 Forecasting

In this section, we compare the performance of the DNS model and the DNS-FR model in out-of-sample forecasting, using the methods discussed in Section 6. Forecast accuracy is evaluated using the RMSE for 12-step ahead ($h = 12$) forecasts.

https://doi.org/10.1017/S174849952610027X Published online by Cambridge University Press

Table 3. 12-step ahead forecasting RMSE for the DNS model

Maturity	UK	FR	IT	DE	JP	AU	EU	US
1 month	0.6645	0.1348	0.2305	0.0698	0.0639	0.5642	0.1164	1.5016
3 months	0.6158	0.0543	0.2390	0.0687	0.0585	0.5202	0.0574	1.4229
6 months	0.5456	0.0724	0.2657	0.1169	0.0510	0.4678	0.0796	1.3378
9 months	0.5257	0.0969	0.2817	0.1718	0.0435	0.4285	0.1203	1.2959
1 year	0.4797	0.0662	0.3215	0.2097	0.0346	0.4075	0.1537	1.2309
2 years	0.4659	0.0541	0.4272	0.1702	0.0317	0.3174	0.0994	1.1570
3 years	0.4744	0.1127	0.5100	0.1073	0.0350	0.3259	0.0652	1.1464
5 years	0.5096	0.2305	0.5819	0.0721	0.0356	0.2357	0.1444	1.1109
7 years	0.4605	0.2481	0.6054	0.0970	0.0558	0.1184	0.2012	0.9822
10 years	0.3946	0.1886	0.5505	0.0783	0.1137	0.1576	0.1798	0.8818
20 years	0.1243	0.1984	0.4190	0.1188	0.4541	0.8816	0.1665	0.5196
30 years	0.1224	0.3753	0.4180	0.2515	0.6326	1.3228	0.1251	0.3364
Mean	0.4486	0.1527	0.4042	0.1277	0.1342	0.4790	0.1258	1.0770

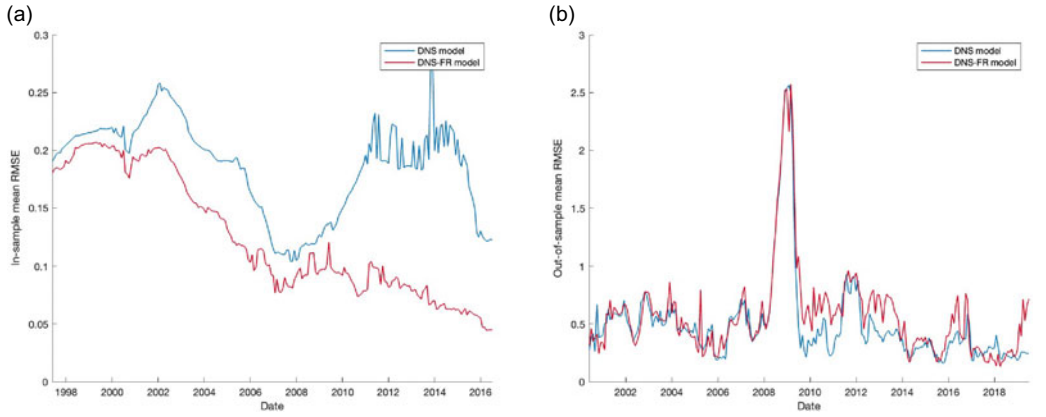
Table 4. 12-step ahead forecasting RMSE for the DNS-FR model

Maturity	UK	FR	IT	DE	JP	AU	EU
1 month	0.7252	0.1168	0.5875	0.1389	0.5606	0.9644	0.1422
3 months	0.6624	0.0722	0.6008	0.1475	0.5646	0.9418	0.0718
6 months	0.5646	0.1130	0.6271	0.1464	0.5688	0.9130	0.0846
9 months	0.5482	0.1336	0.6608	0.1254	0.5684	0.8896	0.1264
1 year	0.5093	0.1150	0.6893	0.1323	0.5734	0.8992	0.1586
2 years	0.4720	0.0862	0.7953	0.1639	0.5442	0.7814	0.1042
3 years	0.4860	0.0787	0.8922	0.2051	0.5148	0.7346	0.0527
5 years	0.5358	0.1996	0.8578	0.2234	0.4452	0.5133	0.1345
7 years	0.5288	0.1967	0.8045	0.2245	0.4137	0.2970	0.2128
10 years	0.5026	0.1437	0.6503	0.1679	0.3622	0.0862	0.1681
20 years	0.1794	0.3798	0.4682	0.1488	0.1159	0.7989	0.1601
30 years	0.1464	0.6761	0.5102	0.2830	0.2720	1.2561	0.2321
Mean	0.4884	0.1926	0.6787	0.1756	0.4587	0.7563	0.1373

Tables 3 and 4 present the RMSE for the DNS model and the DNS-FR model, respectively. Interestingly, for all countries/regions, the DNS model provides a lower mean RMSE than the DNS-FR model. However, it is important to recall that, in the DNS-FR model forecasting process described in Section 6, we first forecast the yields of the reference country (US Treasury) using the DNS model. In Table 3, the mean RMSE for the US Treasury yield prediction is notably high, at least double that of the mean RMSE for other countries/regions. Consequently, the reconstructed factors $\hat{\boldsymbol{U}}_{N+1}, \ldots, \hat{\boldsymbol{U}}_{N+h}$ may not accurately reflect the US Treasury market during this period.

To further compare the performance of the DNS model and the DNS-FR model, we conduct a moving window analysis. The moving window is set as follows: we start with a 5-year window from January 2010 to December 2014, treating this period as in-sample data to estimate model parameters and hidden state variables. We then estimate the yields and calculate the mean RMSE over all maturities and data points within this window. Next, we forecast the yields 12 steps ahead, treating the next 12 months (i.e., from January 2015 to December 2015) as out-of-sample data, and calculate the mean RMSE. We then shift the window forward by one month (i.e., one data point) and repeat the calculations, continuing this process until the last available data point.

https://doi.org/10.1017/S174849952610027X Published online by Cambridge University Press



In-sample mean RMSE. Out-of-sample mean RMSE.

Figure 5. In-sample and out-of-sample mean RMSE for UK yields using a 5-year moving window, move forward for 1 month each time. Each point corresponds to the midpoint of the window, with RMSE averaged over the full window.

Figure 5 shows the in-sample (left) and out-of-sample (right) mean RMSE for UK yields using a moving window. The blue curve represents the mean RMSE for the DNS model, while the red curve represents the mean RMSE for the DNS-FR model. The date of each point corresponds to the midpoint of the window. From the in-sample estimation, it is evident that the DNS-FR model consistently outperforms the DNS model over the entire sample period from 1998 to 2016, with the performance gap widening after 2010. In contrast, for the out-of-sample forecasting, the two curves frequently intersect. During certain periods, such as around 2018, the DNS-FR model achieves a lower mean RMSE, whereas in other periods, notably between 2010 and 2014, the DNS model performs better. Additionally, the differences between the two curves are limited, indicating that both models have similar forecasting performance. The same figures for other countries/regions are provided in Appendix D, and similar conclusions are drawn for all other countries/regions.

8.4 Assessing overfitting in the DNS-FR model

In Sections 8.1, 8.2, and 8.3, we demonstrate that the DNS-FR model outperforms the DNS model in in-sample estimation. However, for out-of-sample prediction, the DNS-FR model exhibits only comparable predictive power in some countries. This raises concerns about potential overfitting. In this section, we address this issue by comparing the DNS-FR model with the following model:

$$Y_t(\tau_i) = F_{1,t} + F_{2,t}\left(\frac{1-e^{-\lambda\tau_i}}{\lambda\tau_i}\right) + F_{3,t}\left(\frac{1-e^{-\lambda\tau_i}}{\lambda\tau_i} - e^{-\lambda\tau_i}\right) + \beta_{\tilde{\tau}} Y_t^{(r)}(\tilde{\tau}) + \epsilon_t(\tau_i) \tag{48}$$

$$F_{j,t} = \psi_{j,0} + \psi_{j,1} F_{j,t-1} + \eta_{j,t}. \tag{49}$$

Here, $Y_t^{(r)}(\tilde{\tau})$ denotes the bond yield of the reference country for a given maturity $\tilde{\tau}$, and $\beta_{\tilde{\tau}}$ is the corresponding coefficient. Unlike the DNS-FR model, Equations (48) and (49) do not incorporate a functional component. Instead, they assume that a simple addition of the reference country's bond yield enhances the DNS model. We refer to this model as the DNS-Reg$X$ model, where X represents the maturity (in months) of the reference bond yield.

Tables E.1 to E.4 in Appendix E present the in-sample estimation errors and out-of-sample forecasting errors. The response yield is the UK bond yield, while the reference yield is the US Treasury yield at six maturities: 1 month, 12 months, 24 months, 60 months, 120 months, and

https://doi.org/10.1017/S174849952610027X Published online by Cambridge University Press

360 months. We also compare the DNS-FR model with different numbers of factors (shown in brackets) extracted.

Table D.1 reports the in-sample estimation errors across different models. Incorporating a single US Treasury maturity into the DNS model reduces the RMSE, with longer maturities offering greater improvements in estimating UK bond yields. However, all variations of the DNS-Reg*X* model yield higher RMSEs than the DNS-FR model, particularly for middle and long-term maturities. This is because the kPCA decomposition captures the level, slope, and curvature dynamics of the US Treasury yield curve, whereas a single time series of US Treasury yields cannot fully represent these features. As a result, although adding a single US Treasury maturity improves the estimation, the functional regression component remains crucial for achieving superior performance. Increasing the number of kPCA factors from 3 to 6 has only a limited impact on in-sample accuracy. For the DNS-FR model with 6 factors, the mean RMSE is 0.0655, approximately 60% lower than that of the DNS model and 37% lower than that of the DNS-Reg360 model.

For out-of-sample forecasting, we consider three settings: a rolling window of 1-step ahead forecasting over the next 12 months (Table D.2), 2-step ahead forecasting (Table D.3), and 12-step ahead forecasting (Table D.4). Overall, the DNS-FR model outperforms both the DNS and DNS-Reg*X* models over longer horizons, while DNS-Reg*X* models achieve lower RMSEs in the short term. For 1-step ahead forecasting, the DNS-Reg120 model achieves the lowest RMSE of 0.1411. In contrast, the best-performing DNS-FR specification, which uses 4 factors, yields an RMSE of 0.1923, around 20% higher than that of the DNS model and 36% higher than the DNS-Reg120 model. This indicates that the functional regression model has limited predictive power over short horizons.

However, for 2-step and 12-step ahead forecasting, the DNS-FR model demonstrates strong predictive performance. In the 2-step ahead setting, the DNS-FR model with 5 factors performs best, with an RMSE of 0.2038, 25% lower than that of the DNS model (0.2709) and 3% lower than the DNS-Reg360 model (0.2108). In the 12-step ahead setting, the best-performing model is the DNS-FR with 6 factors, achieving an RMSE of 0.3275, which is approximately 27% lower than the DNS model and 14% lower than the DNS-Reg360 model. Although the DNS-FR model with 3 factors yields higher forecasting errors than the DNS and DNS-Reg*X* models, increasing the number of kPCA factors leads to substantial improvements in forecasting accuracy over longer horizons, including 2-step forecasts. This suggests that the DNS-FR model does not suffer from overfitting when applied to UK bond yield data.

Figure 6 presents the RMSE of 12-step-ahead forecasts for each tenor of UK bond yields. A 5-year moving window (beginning in January 2010) is employed to fit the model, with the window advancing by one month at each iteration. RMSE values are computed across all windows for each forecast step. For the 2-, 3-, 5-, and 7-year maturities, the DNS-FR model with six factors consistently outperforms the other two models across all forecast steps. In contrast, for the 1-month, 3-month, and 10-year maturities, the DNS-FR model exhibits a larger RMSE than the DNS and DNS-Reg360 models only at a few forecast steps. For the 6-month, 9-month, and 1-year maturities, performance varies across the models. At some steps, the DNS-FR model performs better, while at other steps, the DNS and DNS-Reg360 models yield superior forecasts. For the 20-year and 30-year maturities, the DNS-FR model underperforms relative to the DNS-Reg360 model but achieves a lower RMSE than the DNS model.

Figure 7 displays the mean RMSE across all tenors for the three models. The DNS-FR model with six factors consistently achieves the smallest mean RMSE across all forecast steps, while the DNS model records the largest. The DNS-Reg360 model performs better than the DNS model but still exhibits a larger mean RMSE than the DNS-FR model.

In the remainder of this paper, we focus on the DNS-FR model with 3 factors, despite the 6-factor model demonstrating superior predictive accuracy. This choice is motivated by the fact that the 3-factor model achieves comparable in-sample estimation accuracy while involving significantly fewer parameters.

https://doi.org/10.1017/S174849952610027X Published online by Cambridge University Press

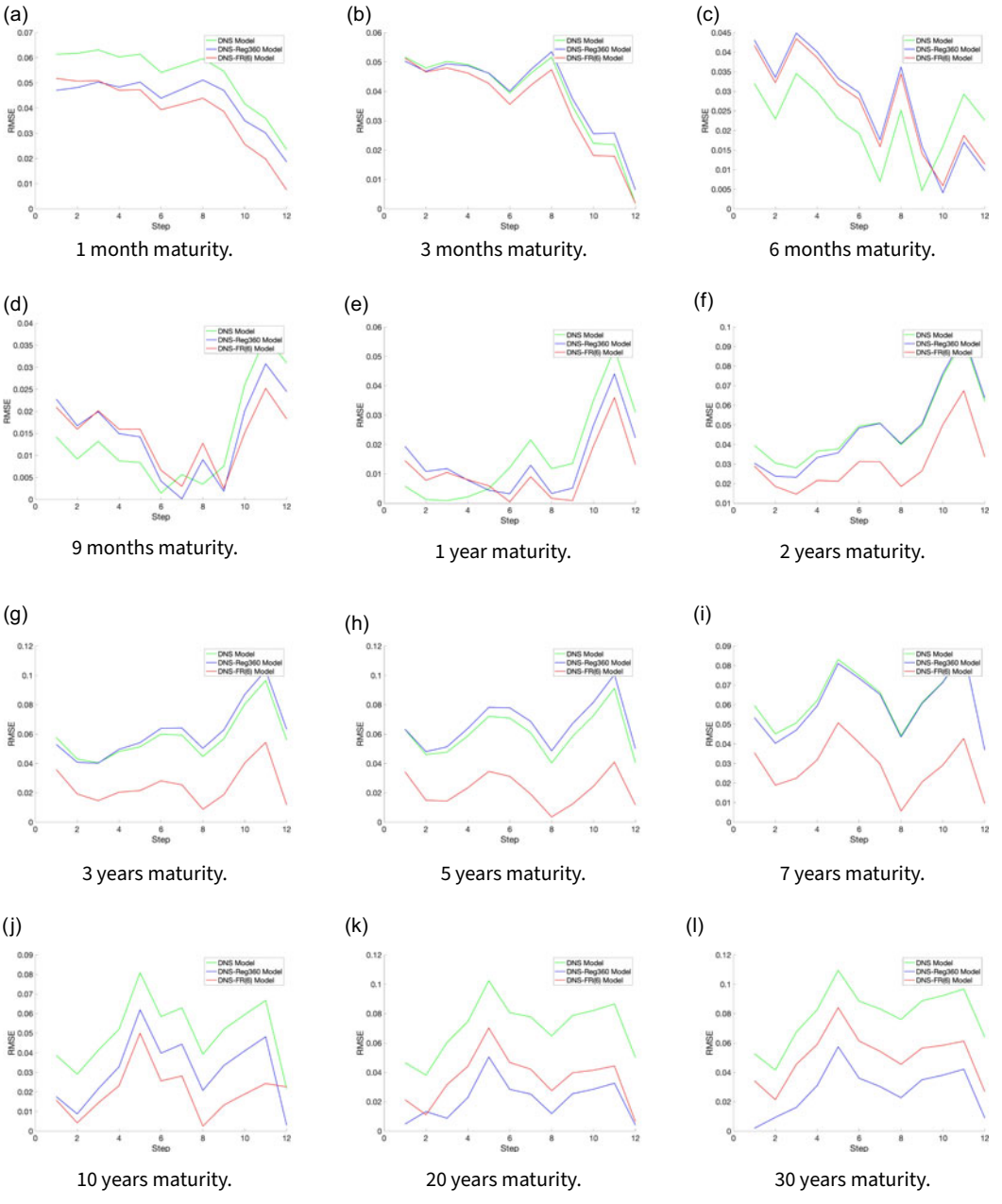


Figure 6. RMSE of 5-year moving window for out-of-sample prediction over 12 steps for each tenor of UK bond yields. The window moves forward for 1 month each time. Results are shown for the DNS model (green), DNS-Reg360 model (blue), and DNS-FR model with 6 factors (red).

8.5 Stress testing

In this section, we conduct a stress testing analysis to answer the following question: If different shocks are applied to the US Treasury market, how do the bond markets of other countries/regions respond? We define two types of stress testing scenarios, each with four cases:

https://doi.org/10.1017/S174849952610027X Published online by Cambridge University Press

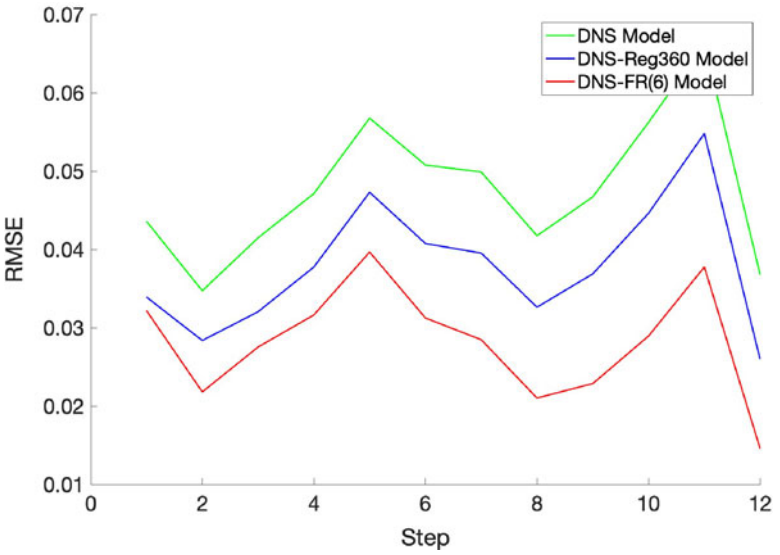


Figure 7. Mean RMSE of 5-year moving window for out-of-sample prediction. The mean value is taken over all maturities.

- Scenario 1: Temporary shocks (January 2015 to December 2015).
  - Case 1.1: Short-end maturities (1, 3, 6, 9 months, and 1, 2, 3, 5 years) yield double.
  - Case 1.2: Middle maturities (7 and 10 years) yield double.
  - Case 1.3: Long-end maturities (20 and 30 years) yield double.
  - Case 1.4: Entire yield curve doubles.
- Scenario 2: Permanent shocks (beginning January 2015).
  - Case 2.1: Short-end maturities (1, 3, 6, 9 months, and 1, 2, 3, 5 years) yield double.
  - Case 2.2: Middle maturities (7 and 10 years) yield double.
  - Case 2.3: Long-end maturities (20 and 30 years) yield double.
  - Case 2.4: Entire yield curve doubles.

To estimate the yields of the response countries, we first apply each stress testing scenario to the US Treasury yield curve. The time series of the US Treasury yields under different stress testing scenarios is provided in Appendix F. Using the amended US Treasury data, we extract kPCA factors. For consistency, we use three factors in this study, with the estimated hyperparameter ι for each scenario listed in Table 5. Finally, we estimate the yields of the response countries.

Figures 8 and 9 show the mean difference in in-sample estimation for UK yields under temporary and permanent shock scenarios, respectively, compared to the estimation under original US Treasury data. Each sub-figure corresponds to cases 1.1 to 1.4 and 2.1 to 2.4. We categorize bonds into three classes: short-end ($(0, 5]$ years), middle ($(5, 10]$ years), and long-end ($(10, 30]$ years). The mean value is taken over all maturities in each class at each time point. The dashed lines represent the lower and upper bounds of the 95% confidence interval,[4] while the vertical black lines indicate the start and end of the shock period for the temporary shocks.

[4]The confidence interval is calculated numerically. We first simulate $n = 1000$ samples from the distribution $\boldsymbol{X}_t|\boldsymbol{Z}_{1:t} \sim N(\boldsymbol{a}_t, \boldsymbol{P}_t)$ at each time point t using the original US yields and the yields in each stress testing scenario, where $\boldsymbol{a}_t$ and $\boldsymbol{P}_t$ are given in Equations (35) and (36). Then, we calculate the estimated yields by $\boldsymbol{Y}_t = \boldsymbol{\Lambda}\boldsymbol{X}_t + \boldsymbol{\Lambda}\boldsymbol{\mu} + \boldsymbol{\Gamma}\boldsymbol{U}_t$. The lower and upper bounds of the confidence interval are the 2.5th and 97.5th percentiles of the mean difference when using the original US data and each stress testing data.

https://doi.org/10.1017/S174849952610027X Published online by Cambridge University Press

Table 5. Estimated hyperparameter ι using 3 factors for different stress testing cases

Stress testing cases	Estimated ι
Original data	0.083
Stress testing 1, case 1.1	0.091
Stress testing 1, case 1.2	0.080
Stress testing 1, case 1.3	0.115
Stress testing 1, case 1.4	0.081
Stress testing 2, case 2.1	0.059
Stress testing 2, case 2.2	0.096
Stress testing 2, case 2.3	0.183
Stress testing 2, case 2.4	0.037

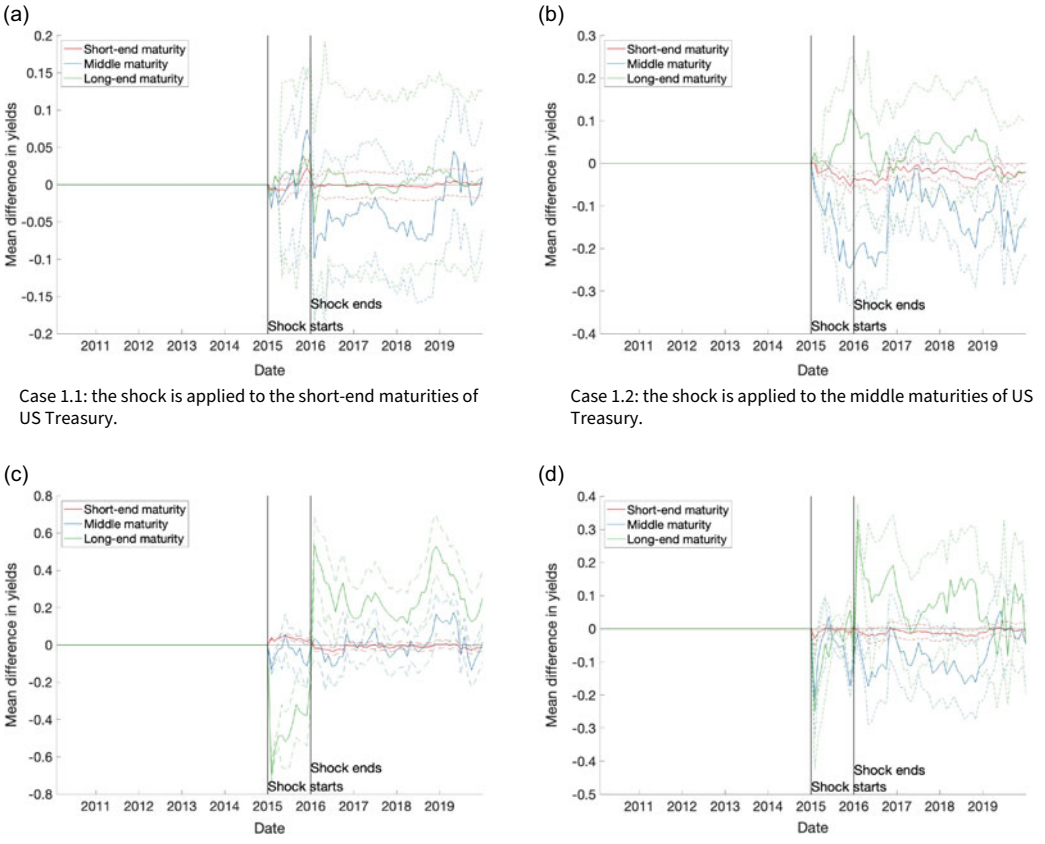
We first consider the effects of the temporary shocks in Figure 8. When the shock is applied to the short-end maturities of the US Treasury yield curve (case 1.1), the effect on UK yields is limited. The confidence intervals cover 0 at almost all time points for all three classes. The short-end maturities of UK yields may have some changes during the shock, but will return to normal levels once the shock ends. When the shock is applied to the middle maturities of the US Treasury (case 1.2), there is a statistically significant effect on the short-end and middle maturities of UK yields. The long-end maturities of UK yields are not affected. Interestingly, even though the shock ended in December 2015, the effects persist in the long run. In case 1.3, when the shock is applied to the long-end maturities of the US Treasury, the entire yield curve is affected, but the long-end maturities are most impacted. Even after the shock, the mean differences in the estimation of long-end maturities remain significantly away from 0. Finally, in case 1.4, when the shock is applied to the entire US Treasury yield curve, the mean differences in the estimation of middle maturities of UK yields are affected in some intervals, for example, from July 2015 to September 2016, and from September 2017 to December 2019, while neither the short nor the long maturities exhibit a significant effect.

One should note that for the temporary shock, even though it ended in December 2015, some maturities of UK yields are still affected in the long run in some cases, such as the middle maturities in case 1.2 and the long-end maturities in case 1.3. This can be explained as follows. In a regression model, the change in the covariate at time t only affects the response variable at time t. However, if the covariate is autoregressive, the change in the covariate at time t will be accumulated over a long period.

Now, we move on to the permanent shock in Figure 9. Unlike the temporary shock, a permanent shock usually does not affect the UK yields in the long run. During the first few months after the shock starts, all the short-end, middle, and long-end maturities of UK yields react to this shock. However, after that, the yield curve returns to normal levels and fluctuates in the short run. The permanent shock affects the middle and long-end maturities more than the short-end maturities in all four cases.

Another notable feature is the green peaks almost immediately after the shocks start in cases 1.3/2.3 and 1.4/2.4 in Figures 8 and 9. This indicates that whenever a temporary or permanent shock is applied to the long-end maturities or the entire US Treasury yield curve, the long-end maturities of UK bonds react immediately. However, the UK bond market may overreact to this shock. Subsequently, the effects of this shock decrease, and the yields return to normal levels in a few months. If the shock is temporary, when it ends, the UK bond market, especially the

https://doi.org/10.1017/S174849952610027X Published online by Cambridge University Press



Case 1.1: the shock is applied to the short-end maturities of US Treasury.

Case 1.2: the shock is applied to the middle maturities of US Treasury.

Case 1.3: the shock is applied to the long-end maturities of US Treasury.

Case 1.4: the shock is applied to allmaturities of US Treasury.

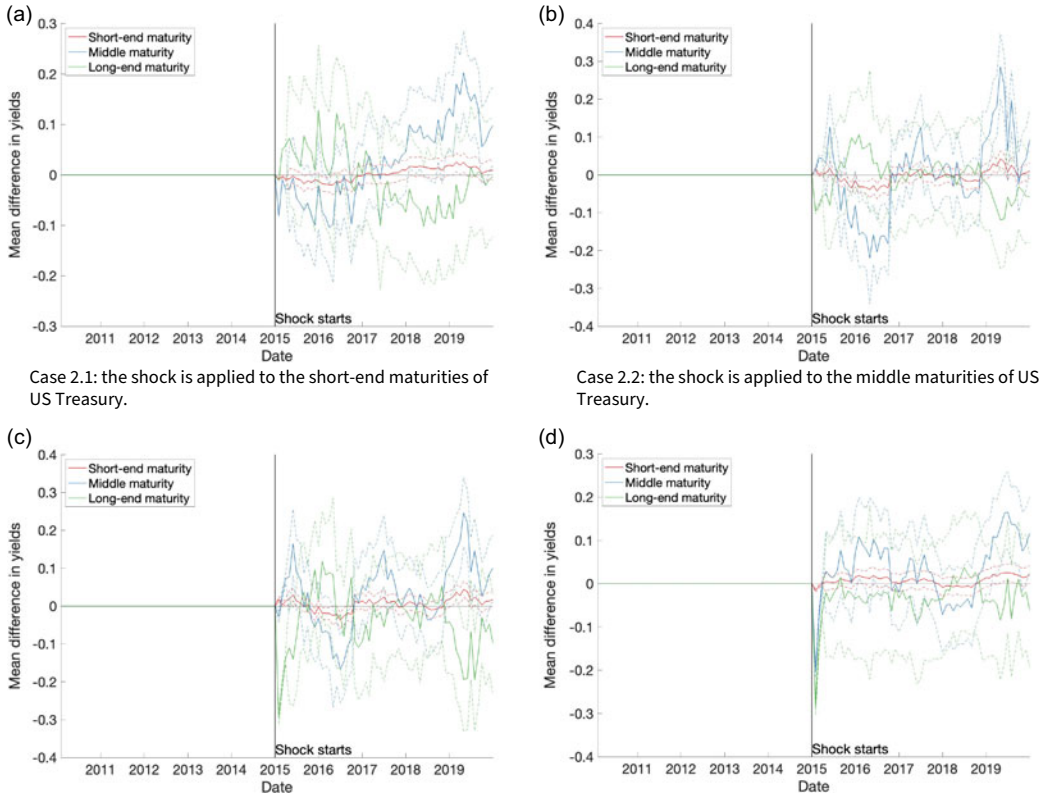
Figure 8. Mean difference in percentage points of in-sample estimations between stress testing scenario 1 and original data for UK yields. The mean values are taken over short-end ((0, 5] years), middle ((5, 10] years), and long-end ((10, 30] years) maturities. Dashed lines represent the lower and upper bounds of 95% confidence interval for each curve.

long-end maturities, will overreact again. This is because, in our stress testing setup, when a temporary shock ends, the US Treasury yields are halved, causing another dramatic change in the US Treasury yield curve.

Finally, Figure 10 provides the estimated functional coefficients for the UK yields for the original US Treasury data, stress testing scenario 1 data, and stress testing scenario 2 data. For the stress testing data, we only consider cases 1.4 and 2.4, i.e., shocks applied to the entire yield curve. In each sub-figure, different colors represent different functional coefficients $\gamma_i(\tau)$ for $i \in \{1, \ldots, 12\}$, in Equation (8).

For the original US Treasury data, the long-end maturities of UK bonds are mostly affected by the long-end maturities of the US Treasury ($\gamma_{11}(\tau), \gamma_{12}(\tau)$), while the middle maturities of UK bonds are mostly affected by the middle maturities of the US Treasury ($\gamma_9(\tau), \gamma_{10}(\tau)$). All other maturities are evenly affected by the entire US Treasury yield curve. When a temporary shock is applied to the US Treasury, these relationships change slightly. The long-end maturities of UK bonds are still affected by the long-end maturities of the US Treasury, but they are also affected by the 1-year, 2-year, and 3-year US Treasury. The effects of the middle maturities of the US Treasury decrease. All other UK bonds with maturities less than or equal to 10 years are evenly affected by the entire US Treasury yield curve. As for the permanent shock, the effects

https://doi.org/10.1017/S174849952610027X Published online by Cambridge University Press



Case 2.1: the shock is applied to the short-end maturities of US Treasury.

Case 2.2: the shock is applied to the middle maturities of US Treasury.

Case 2.3: the shock is applied to the long-end maturities of US Treasury.

Case 2.4: the shock is applied to allmaturities ofUS Treasury.

Figure 9. Mean difference in percentage points of in-sample estimations between stress testing scenario 2 and the original data for UK yields. The mean values are taken over short-end ((0, 5] years), middle ((5, 10] years), and long-end ((10, 30] years) maturities. Dashed lines represent the lower and upper bounds of 95% confidence interval for each curve.

of the long-end maturities of the US Treasury disappear. Instead, the middle maturities of the US Treasury contribute more to the UK bonds, especially the middle maturities of UK bonds $(\gamma_8(\tau), \gamma_9(\tau), \gamma_{10}(\tau))$.

8.6 Case study: Bond ladder portfolio

In this section, we present a case study of a bond ladder portfolio for risk management purposes. A bond ladder portfolio can be described as follows. Assume a US investor wants to construct an investment strategy consisting of cash and a UK bond with a maturity of T months. At time t_i, the investor spends p_i dollars to purchase bonds and deposits the remaining amount in a bank account. We denote the number of bonds as N_i and the value of the portfolio at time t_i as W_i for $i \in \{0, 1, \ldots, k\}$. The initial wealth W_0 is 12 million USD. For simplicity, we assume $p_1 = p_2 = \cdots = p$, meaning the investor spends the same amount on bonds each month. The value of the portfolio W_t can be calculated as follows, assuming the interest rate is compounded monthly, and the investment interval is one month:

$$W_i = \sum_{j=0}^{k} N_j F_i e^{-\tau_j Y_i(\tau_j)} \mathbf{1}_{\{t_j \le t_i, \tau_j \ge 0\}} + \left(1 + \frac{r_i}{12}\right) C_{i-1} \tag{50}$$

https://doi.org/10.1017/S174849952610027X Published online by Cambridge University Press

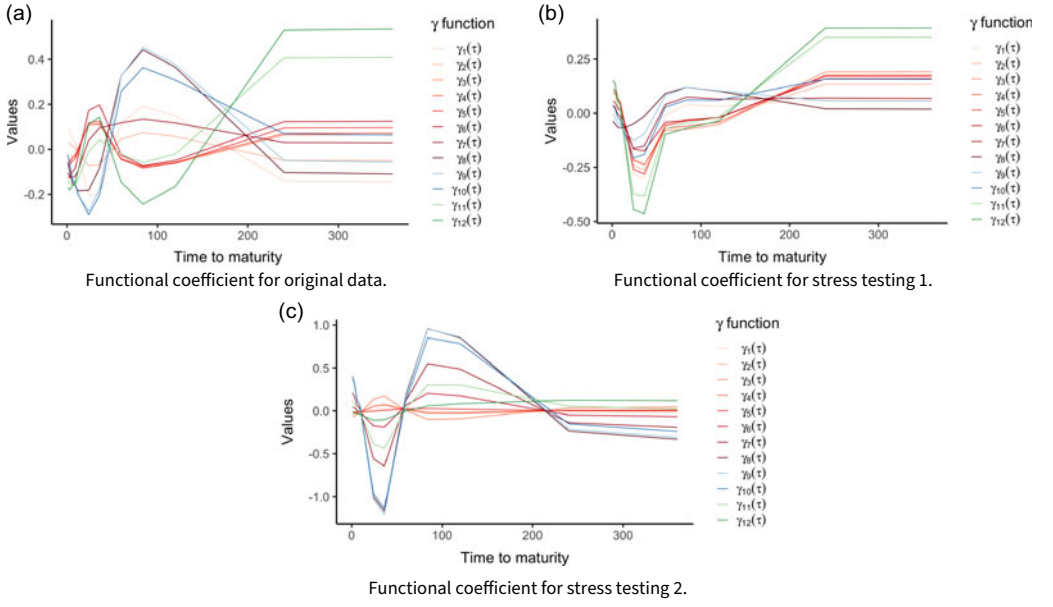


Figure 10. Functional coefficients for UK yields.

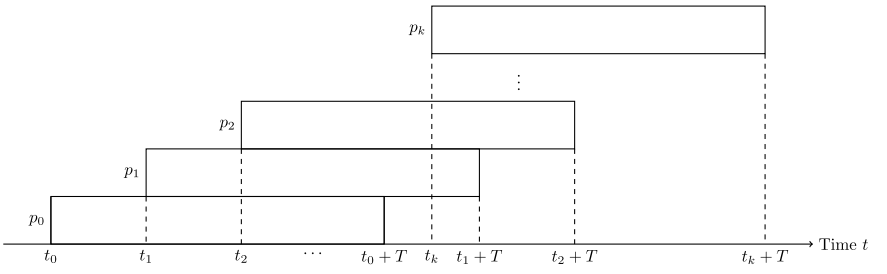


Figure 11. Construction of a bond ladder portfolio.

where F_i is the face value in USD at time t_i,[5] r_i is the risk-free interest rate[6] for the period $[t_{i-1}, t_i]$, $\mathbf{1}_{\{\cdot\}}$ is the indicator function, and C_{i-1} is the amount in the cash account at time t_{i-1}. The number of bonds N_j is calculated as:

$$N_j = \frac{p}{F_j e^{-TY_j(T)}}. \tag{51}$$

Figure 11 illustrates the entire process of constructing the bond ladder portfolio.

In this study, we assume the investor makes 13 investments ($k+1=13$) over one year, from December 2019 to December 2020. The effective federal funds rate (EFFR) data and the GBP/USD exchange rate[7] for this period are given in Table 6. Furthermore, we assume the bond yield for

[5]The face value in GBP is usually a constant. However, as the GBP/USD exchange rate changes over time, the face value in USD also changes.

[6]In this paper, we used the EFFR as a proxy for the risk-free interest rate. The EFFR data was sourced from the website of the Federal Reserve Bank of New York. Although the original data are provided on a daily basis, we converted them to monthly data for consistency.

[7]Data were obtained from https://www.tradingview.com/.

https://doi.org/10.1017/S174849952610027X Published online by Cambridge University Press

Table 6. Monthly EFFR data and the GBP/USD exchange rate for the year 2020

Date	EFFR	GBP/USD exchange rate
December 2019	–	1.32018
January 2020	1.59%	1.28231
February 2020	1.59%	1.24086
March 2020	0.08%	1.25907
April 2020	0.05%	1.23455
May 2020	0.05%	1.23992
June 2020	0.08%	1.30770
July 2020	0.10%	1.33690
August 2020	0.09%	1.29115
September 2020	0.09%	1.29457
October 2020	0.09%	1.33173
November 2020	0.09%	1.36561
December 2020	0.09%	1.36893

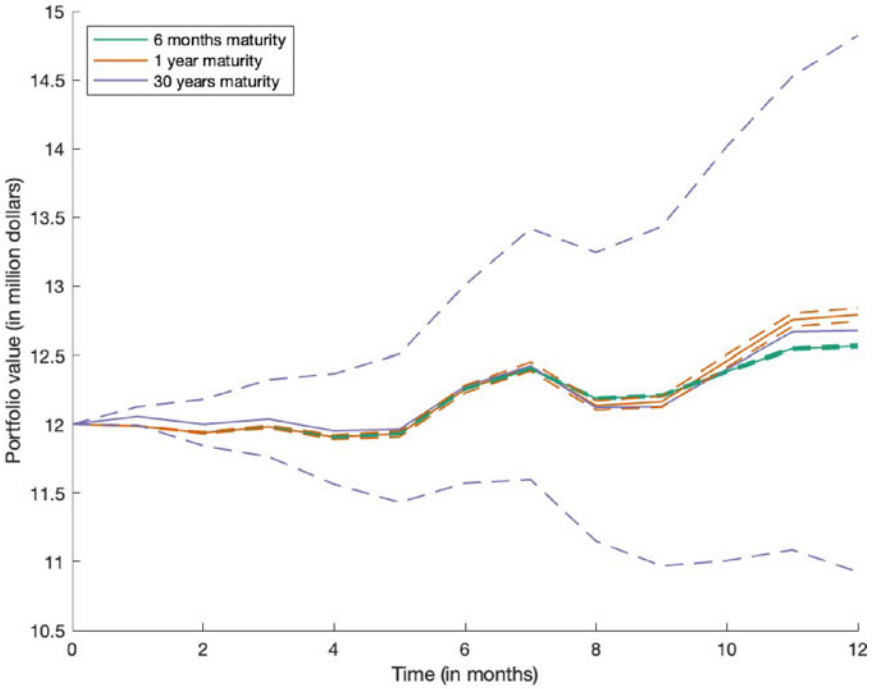


Figure 12. Predicted portfolio values.

the first investment (made in December 2019) is known, while the yields for the subsequent 12 investments are predicted using the DNS-FR model.[8] We consider three main questions:

1. How does the value of the portfolio change over time?
2. How do different stress tests affect the value of the portfolio?

[8]In this case study, the time to maturity τ_i can take any integer between 1 and T. However, we only know the coefficients $\gamma_{i,j}$ at $\tau_i = 1, 3, 6, 9$ months, and 1, 2, 3, 5, 7, 10, 20, and 30 years. In this case, we first forecast the yields at those points, then take a linear interpolation to fill all the values between any two points.

https://doi.org/10.1017/S174849952610027X Published online by Cambridge University Press

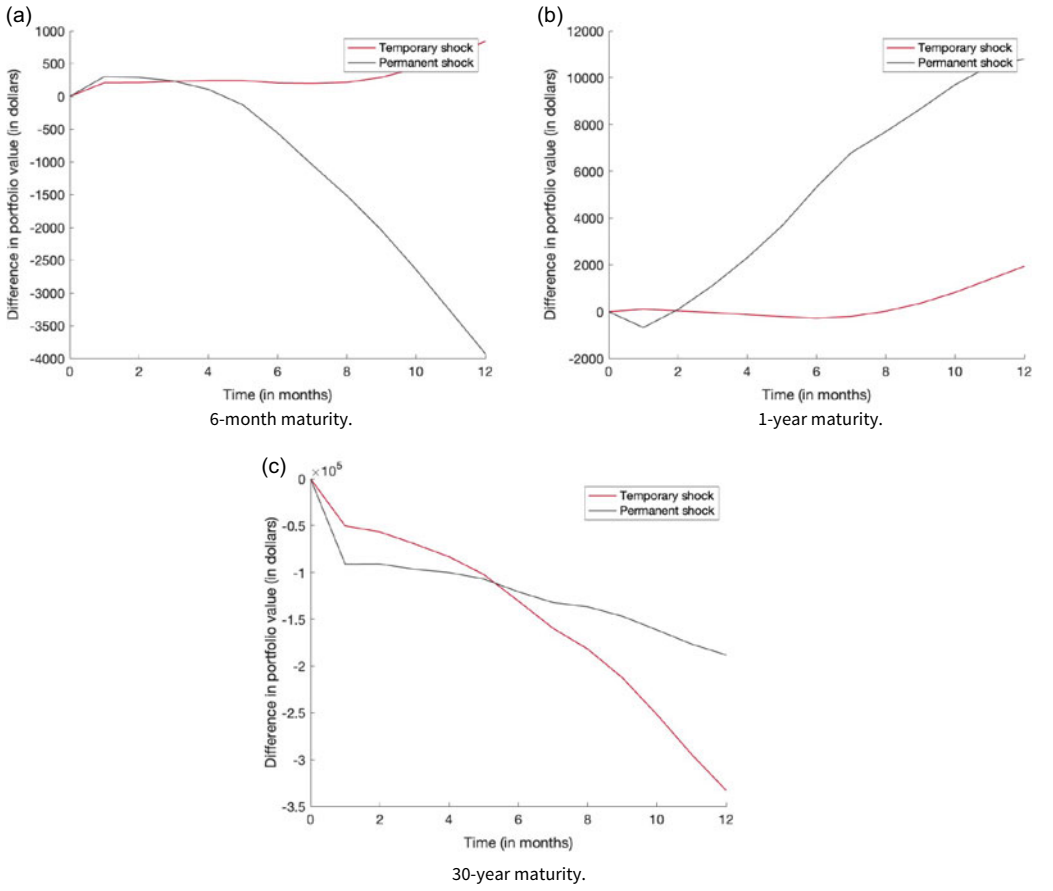


Figure 13. Differences in portfolio values between each stress testing scenario and the original data, for different maturities of the underlying bond.

3. How does the value of the portfolio change with different maturities of the underlying bond?

For the second question, we consider the stress testing scenarios 1.4 and 2.4 described in Section 8.5, i.e., the shocks are applied to the entire yield curve. For the third question, we consider three different bonds with maturities of 6 months, 1 year, and 30 years, respectively.

Figure 12 shows the predicted portfolio values for the next 12 months for underlying bonds with maturities of 6 months, 1 year, and 30 years. The monthly investment amount is $1 million for all maturities. For the first five months, the portfolio values of all bonds are lower than the initial wealth of $12 million, mainly due to the decrease in the exchange rate. This also explains the decreases in portfolio values in the 8th and 9th months. At the end of 12 months, the 1-year bond has the maximum predicted portfolio value, followed by the 30-year bond, and the 6-month bond has the minimum predicted portfolio value. However, the differences among the three bonds are small. Another notable observation is that as maturities increase, so does risk. For example, at the end of 12 months, the portfolio value of the 6-month bond is roughly $12.5 million with no uncertainty, while the portfolio value of the 30-year bond could be as high as $14.5 million or as low as $11 million, reflecting the common understanding that long-term debt usually carries higher risk.

https://doi.org/10.1017/S174849952610027X Published online by Cambridge University Press

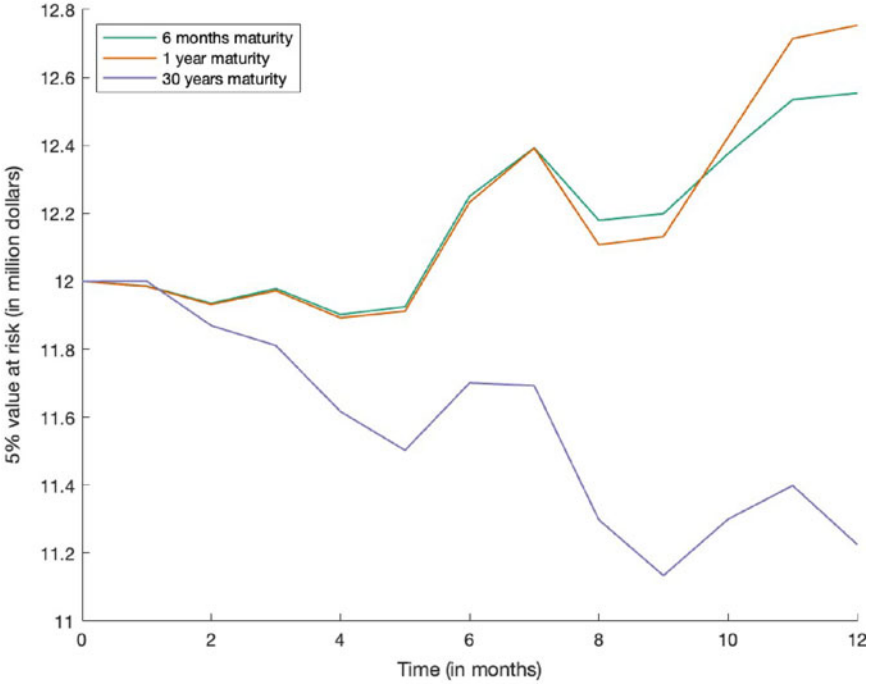


Figure 14. 5% value-at-risk (VaR) for bond ladder portfolios with different maturities.

Figure 13 illustrates the differences in portfolio values between different shocks and the original data for the 6-month, 1-year, and 30-year bonds, respectively. A positive value indicates that the portfolio is worth more under the shock, while a negative value indicates that it is worth less. For short-end maturities (6-month and 1-year), the temporary shock has limited effects, but the permanent shock significantly impacts portfolio values. However, for the long-end maturity (30-year), the opposite is true. The permanent shock in 2015 has a larger effect on the portfolio values. Although this shock dissipated by the end of 2015, it continues to affect the long-end curve over an extended period.

In reality, VaR also attracts considerable attention. People are particularly concerned with the maximum potential loss under normal market conditions after excluding the worst outcomes with a total probability of p%. Figure 14 shows the 5% VaR for the portfolio value of bonds with 6-month, 1-year, and 30-year maturities, which is calculated numerically. At the end of 12 months, the 5% VaR of the portfolio values of the 6-month and 1-year bonds are roughly \$12.5 and \$12.7 million, respectively, indicating a minimal chance of loss with these bonds even in the worst cases. In contrast, the 5% VaR of the portfolio value of the 30-year bond is only about \$11.2 million, suggesting that investing in a 30-year bond could lead to a loss over a 1-year period in the worst case.

Figure 15 shows the difference in 5% VaR between each stress testing scenario and the original US Treasury data for different maturities of UK bonds. Overall, if a shock is applied to the US Treasury, the 5% VaR of the portfolio value of UK bonds will decrease. For the 6-month bond, both the temporary shock and the permanent shock have a similar effect on 5% VaR. For the 1-year bond, the permanent shock has a limited effect on 5% VaR, while the temporary shock has a significant influence. For the 30-year bond, both temporary and permanent shocks have a substantial influence on 5% VaR, with the influence of the temporary shock being stronger. Another notable feature is the magnitude of the difference in 5% VaR. For the 6-month bond, a shock can cause a decrease in 5% VaR up to \$7,000 at the end of 12 months, while for the

https://doi.org/10.1017/S174849952610027X Published online by Cambridge University Press

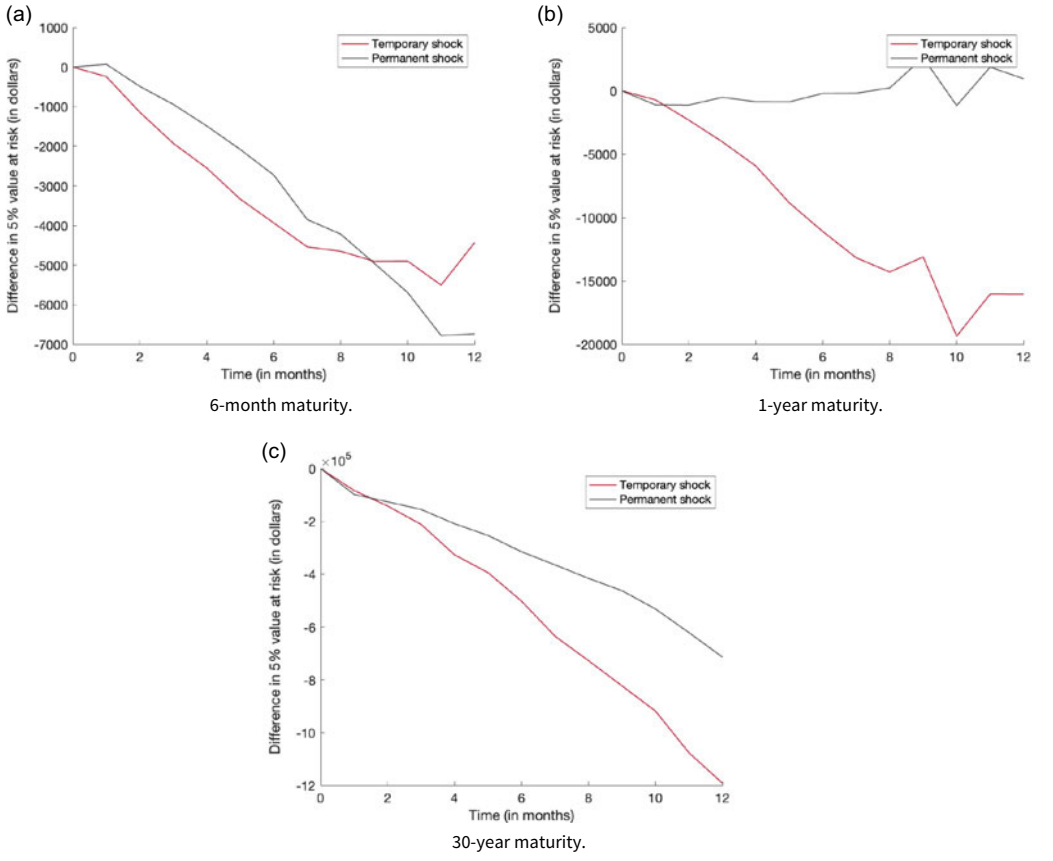


Figure 15. Differences of 5% value-at-risk (VaR) between each stress testing scenario and the original data, for different maturities of the underlying bond.

30-year bond, a temporary shock causes a decrease of $\$1,200,000$ in 5% VaR. Long-term bonds are more sensitive to the shock.

9. Conclusion

The DNS model has been pivotal in yield curve estimation over the past two decades. However, it falls short in capturing the relative spread between two economies. In this paper, we introduce a novel DNS-FR model, which extends the DNS model by incorporating the relative spread between a reference country and a response country. To address estimation challenges, we use kPCA to transform the functional regression into a finite-dimensional estimation problem. The Kalman Filter method is then employed to estimate unknown parameters and hidden state variables by maximizing the marginal likelihood function.

Our empirical analysis, which includes eight countries/regions with the US as the reference country and seven response countries/regions, demonstrates that the DNS-FR model outperforms the DNS model in in-sample estimation, particularly for long-term bonds with maturities of 20 and 30 years, across all seven response countries/regions. Additionally, the DNS-FR model is superior in capturing unusual yield curve structures, such as local fluctuations and inversions.

Furthermore, we conducted stress tests to analyze the effects of both temporary and permanent shocks applied to the US Treasury yield curve on the estimation of UK bond yields.

https://doi.org/10.1017/S174849952610027X Published online by Cambridge University Press

The study reveals that middle and long-end maturities of UK bonds are mostly affected, regardless of whether the shock is applied to the short-end, middle, or long-end maturities of the US Treasury yield curve. Interestingly, for temporary shocks, their effects persist in the long run even after the shocks end.

Finally, we conducted a case study of a bond ladder portfolio, involving regular investments in UK bonds for risk management purposes. We forecasted the portfolio values 12 steps ahead with 6-month, 1-year, and 30-year bonds. The predicted portfolio values for the three bonds are similar, but the bond with a longer maturity carries higher risk, reflected in a wider confidence interval. The 5% VaR suggests that investing in the 6-month and 1-year bonds is unlikely to result in a loss over one year, whereas investing in the 30-year bond may lead to a loss in the worst-case scenario. Furthermore, we analyzed the influence of different types of shocks on the predicted portfolio values and VaR. The permanent shock has larger effects on short-end maturities, while the temporary shock, even though it ended a few years ago, has a more significant effect on long-end maturities.

Acknowledgements. This study was partially presented at the 68th Euro Working Group for Commodity and Financial Modelling. We would like to thank the audience and organizers for their valuable feedback and suggestions.

Supplementary material. The supplementary material for this article can be found at https://doi.org/10.1017/S174849952610027X

Data availability statement. The original bond yield data were obtained from https://www.tradingview.com/. The authors do not have permission to share the raw data. A sample data and the codes are available on GitHub at: https://github.com/peilun-he/State-Space-Dynamic-Functional-Regression-for-Multicurve.

Funding statement. This work received no specific grant from any funding agency, commercial, or not-for-profit sectors.

Competing interests. All authors declare that they have no competing interests.

Author contributions. Software: Peilun He; Gareth W. Peters; Nino Kordzakhia. Validation: Peilun He. Investigation: Peilun He; Gareth W. Peters; Nino Kordzakhia; Pavel V. Shevchenko. Formal analysis: Peilun He; Gareth W. Peters. Writing – Original Draft: Peilun He; Gareth W. Peters. Writing – Review and Editing: Peilun He; Gareth W. Peters; Nino Kordzakhia; Pavel V. Shevchenko. Visualization: Peilun He. Conceptualization: Gareth W. Peters. Methodology: Gareth W. Peters; Nino Kordzakhia; Pavel V. Shevchenko. Supervision: Gareth W. Peters; Nino Kordzakhia; Pavel V. Shevchenko.

References

Ametrano, **F. M.** & **Bianchetti**, **M.** (2013). Everything you always wanted to know about multiple interest rate curve bootstrapping but were afraid to ask. SSRN Working Paper. Available at: https://ssrn.com/abstract=2219548.

Andersson, **P.** & **Lagerås**, **A. N.** (2013). Optimal bond portfolios with fixed time to maturity. *Insurance: Mathematics and Economics*, **53**(2), 429–438.

Bernard, **C.**, **Le Courtois**, **O.** & **Quittard-Pinon**, **F.** (2005). Market value of life insurance contracts under stochastic interest rates and default risk. *Insurance: Mathematics and Economics*, **36**(3), 499–516.

Bowsher, **C. G.** & **Meeks**, **R.** (2008). The dynamics of economic functions: Modeling and forecasting the yield curve. *Journal of the American Statistical Association*, **103**(484), 1419–1437.

Cairns, **A. J.** (1998). Descriptive bond-yield and forward-rate models for the British government securities' market. *British Actuarial Journal*, **4**(2), 265–321.

Cairns, **A. J.** (2004). *Interest rate models: An introduction*. Princeton University Press.

Cairns, **A. J.** & **Pritchard**, **D. J.** (2001). Stability of models for the term structure of interest rates with application to German market data. *British Actuarial Journal*, **7**(3), 467–507.

Campi, **M.**, **Peters**, **G. W.** & **Richards**, **K.-A.** (2024). Shades of green: Unveiling the impact of municipal green bonds on the environment. *Franklin Open*, **7**, 100113.

Christensen, **J. H.**, **Diebold**, **F. X.** & **Rudebusch**, **G. D.** (2009). An arbitrage-free generalized Nelson-Siegel term structure model. *Econometrics Journal*, **12**, C33–C64.

https://doi.org/10.1017/S174849952610027X Published online by Cambridge University Press

Cox, **J. C.**, **Ingersoll**, **J. E.**, **Jr.** & **Ross**, **S. A.** (1985). A theory of the term structure of interest rates. *Econometrica*, **53**(2), 385–407.

Diebold, **F. X.** & **Li**, **C.** (2006). Forecasting the term structure of government bond yields. *Journal of Econometrics*, **130**(2), 337–364.

Diebold, **F. X.**, **Li**, **C.** & **Yue**, **V. Z.** (2008). Global yield curve dynamics and interactions: A dynamic Nelson–Siegel approach. *Journal of Econometrics*, **146**(2), 351–363.

Diebold, **F. X.** & **Rudebusch**, **G. D.** (2013). *Yield curve modeling and forecasting: The dynamic Nelson-Siegel approach*. Princeton University Press.

Diebold, **F. X.**, **Rudebusch**, **G. D.** & **Aruoba**, **S. B.** (2006). The macroeconomy and the yield curve: A dynamic latent factor approach. *Journal of Econometrics*, **131**(1–2), 309–338.

Dobbie, **G.** & **Wilkie**, **A.** (1978). The F.T.-actuaries fixed interest indices. *Journal of the Institute of Actuaries*, **105**(1), 15–26.

Dubecq, **S.** & **Gourieroux**, **C.** (2011). An analysis of the ultra long-term yields. SSRN Working Paper. Available at: https://ssrn.com/abstract=1943535.

Duffie, **D.** & **Kan**, **R.** (1996). A yield-factor model of interest rates. *Mathematical Finance*, **6**(4), 379–406.

Eghbalzadeh, **R.**, **Godin**, **F.** & **Gaillardetz**, **P.** (2024). The discrete-time arbitrage-free Nelson-Siegel model: A closed-form solution and applications to mixed funds representation. *Annals of Actuarial Science*, **18**(2), 310–341.

Filipovic, **D.** (1999). A note on the Nelson–Siegel family. *Mathematical Finance*, **9**(4), 349–359.

Fontana, **C.**, **Lanaro**, **G.** & **Murgoci**, **A.** (2025). The geometry of multi-curve interest rate models. *Quantitative Finance*, **25**(2), 323–342.

Fontana, **C.** & **Rotondi**, **F.** (2023). Valuation of general GMWB annuities in a low interest rate environment. *Insurance: Mathematics and Economics*, **112**, 142–167.

Gaillardetz, **P.** (2008). Valuation of life insurance products under stochastic interest rates. *Insurance: Mathematics and Economics*, **42**(1), 212–226.

Guirreri, **S.** (2010). YieldCurve: Modelling and estimation of the yield curve. R package. Available at: https://CRAN.R-project.org/package=YieldCurve.

Günther, **S.** & **Hieber**, **P.** (2024). Analyzing the interest rate risk of equity-indexed annuities via scenario matrices. *Insurance: Mathematics and Economics*, **114**, 15–28.

Han, **N.-W.** & **Hung**, **M.-W.** (2017). Optimal consumption, portfolio, and life insurance policies under interest rate and inflation risks. *Insurance: Mathematics and Economics*, **73**, 54–67.

Hays, **S.**, **Shen**, **H.** & **Huang**, **J. Z.** (2012). Functional dynamic factor models with application to yield curve forecasting. *The Annals of Applied Statistics*, 870–894.

Heath, **D.**, **Jarrow**, **R.** & **Morton**, **A.** (1992). Bond pricing and the term structure of interest rates: A new methodology for contingent claims valuation. *Econometrica: Journal of the Econometric Society*, **60**, 77–105.

Hull, **J.** & **White**, **A.** (1990). Pricing interest-rate-derivative securities. *The Review of Financial Studies*, **3**(4), 573–592.

Hyndman, **R. J.** & **Shang**, **H. L.** (2009). Forecasting functional time series. *Journal of the Korean Statistical Society*, **38**(3), 199–211.

Iacopini, **M.**, **Poon**, **A.**, **Rossini**, **L.** & **Zhu**, **D.** (2024). A quantile Nelson-Siegel model. ArXiv preprint. Available at https://arxiv.org/abs/2401.09874.

Ismayilova, **A.** & **Ismayilov**, **M.** (2024). On the universal approximation property of radial basis function neural networks. *Annals of Mathematics and Artificial Intelligence*, **92**(3), 691–701.

Jiang, **J.** (2014). Multivariate functional-coefficient regression models for nonlinear vector time series data. *Biometrika*, **101**(3), 689–702.

Johnson, **C. R.**, **Neumann**, **M.** & **Tsatsomeros**, **M. J.** (1996). Conditions for the positivity of determinants. *Linear and Multilinear Algebra*, **40**(3), 241–248.

Karimalis, **E.**, **Kosmidis**, **I.** & **Peters**, **G. W.** (2017). Multi yield curve stress-testing framework incorporating temporal and cross tenor structural dependencies. Bank of England Working Paper No. 655. Bank of England. Available at: https://www.bankofengland.co.uk/working-paper/2017/multi-yield-curve-stress-testing-framework-incorporating-temporal-and-cross-tenor-structural.

Koopman, **S. J.**, **Mallee**, **M. I.** & **Van der Wel**, **M.** (2010). Analyzing the term structure of interest rates using the dynamic Nelson–Siegel model with time-varying parameters. *Journal of Business & Economic Statistics*, **28**(3), 329–343.

Martınez-Hernández, **I.**, **Gonzalo**, **J.** & **González-Farıas**, **G.** (2022). Nonparametric estimation of functional dynamic factor model. *Journal of Nonparametric Statistics*, **34**(4), 895–916.

Nelson, **C. R.** & **Siegel**, **A. F.** (1987). Parsimonious modeling of yield curves. *Journal of Business*, **60**, 473–489.

Peng, **X.** & **Li**, **B.** (2023). Optimal investment, consumption and life insurance purchase with learning about return predictability. *Insurance: Mathematics and Economics*, **113**, 70–95.

Peters, **G. W.** & **Loke**, **S.-H.** (n.d.). *Introduction to fixed income markets and bonds [to appear]*. Foundations for Undergraduate Research in Mathematics. Springer.

Schumann, **E.** (2016). NMOF: Numerical methods and optimization in finance. R package. Available at: https://CRAN.R-project.org/package=NMOF.

https://doi.org/10.1017/S174849952610027X Published online by Cambridge University Press

Shawe-Taylor, **J.** & **Cristianini**, **N.** (2004). *Kernel methods for pattern analysis*. Cambridge University Press.

Sriperumbudur, **B. K.**, **Fukumizu**, **K.** & **Lanckriet**, **G. R.** (2011). Universality, characteristic kernels and RKHS embedding of measures. *Journal of Machine Learning Research*, **12**(7), 2389–2410.

Svensson, **L. E.** (1994). Estimating and interpreting forward interest rates: Sweden 1992–1994. NBER Working Paper No. 4871. National Bureau of Economic Research. Available at: https://www.nber.org/papers/w4871.

Szabó, **Z.** & **Sriperumbudur**, **B. K.** (2018). Characteristic and universal tensor product kernels. *Journal of Machine Learning Research*, **18**(233), 1–29.

Toczydlowska, **D.** & **Peters**, **G. W.** (2018). Financial big data solutions for state space panel regression in interest rate dynamics. *Econometrics*, **6**(3), 34.

Vasicek, **O.** (1977). An equilibrium characterization of the term structure. *Journal of Financial Economics*, **5**(2), 177–188.

Wahlstrøm, **R. R.**, **Paraschiv**, **F.** & **Schürle**, **M.** (2022). A comparative analysis of parsimonious yield curve models with focus on the Nelson-Siegel, Svensson and Bliss versions. *Computational Economics*, **59**, 1–38.

Wang, **J.**, **Chen**, **Q.** & **Chen**, **Y.** (2004). RBF kernel based support vector machine with universal approximation and its application. In International Symposium on Neural Networks, pp. 512–517. Springer.

Wang, **P.** & **Li**, **Z.** (2018). Robust optimal investment strategy for an AAM of DC pension plans with stochastic interest rate and stochastic volatility. *Insurance: Mathematics and Economics*, **80**, 67–83.

Yu, **W.-C.** & **Zivot**, **E.** (2011). Forecasting the term structures of treasury and corporate yields using dynamic Nelson-Siegel models. *International Journal of Forecasting*, **27**(2), 579–591.

Cite this article: He P, Peters GW, Kordzakhia N and Shevchenko PV (2026). State-space dynamic functional regression for multicurve fixed income spread analysis and stress testing, *Annals of Actuarial Science*, **20**, 439–472. https://doi.org/10.1017/S174849952610027X

https://doi.org/10.1017/S174849952610027X Published online by Cambridge University Press